Lagrangian studies of marine production: a multi-method assessment of productivity relationships in the California Current Ecosystem upwelling region

Sven Alexander Kranz[1], Seaver Wang[2], Thomas B Kelly[1], Michael R Stukel[1], Ralf Goericke[3], Michael R. Landry[3], and Nicolas Cassar[2]

[1]Florida State University
[2]Duke University
[3]University of California, San Diego

November 25, 2022

Abstract

Upwelling of nutrient rich waters along continental shelves generates highly productive marine ecosystems affectingplanktonic communities from coastal to offshore domains. Methods to constrain pelagic productivity are often based on different physiological or ecosystem processes, hence describe different biogeochemically important processes. Here, we present a multi-method process-oriented investigation of diverse productivity measures in the California Current Ecosystem (CCE) Long-Term Ecological Research study region, a complex physical environment. The data are from seven multi-day deployments over two field expeditions (spring 2016 and summer 2017) and cover a transition region from high to low productivity. Employing a Lagrangian study design, we aimed to follow the water parcels over several days, comparing 24 h in-situ measurements (C and NO, uptake, sediment trap export, dilution estimates of phytoplankton growth and microzooplankton grazing) with high-resolution productivity measurements by Fast Repetition Rate Fluorometry (FRRF) and Equilibrium Inlet Mass Spectrometry (EIMS). Our results show the importance of accounting for temporal and fine spatial scale variability when estimating ecosystem production. FRRF and EIMS measurements resolved diel patterns in gross primary and net community production. Diel productivity changes agreed well with comparable more traditional measurements. While differences in productivity metrics calculated over different time intervals were considerable, as those methods rely on different base assumptions, our data can be used to explain ecosystem processes which would otherwise have gone unnoticed. The processes resolved from this method comparison can help to further our understanding of the coupling and decoupling of surface productivity and potential carbon burial in coastal and offshore ecosystems.

Lagrangian studies of marine production: a multi-method assessment of productivity relationships in the California Current Ecosystem upwelling region

Sven A Kranz[1,*], Seaver Wang[2], Thomas B Kelly[1], Michael R Stukel[1,3], Ralf Goericke[4], Michael R. Landry[4], Nicolas Cassar[2]

[1]Dept. of Earth, Ocean & Atmospheric Sciences, Florida State University, Tallahassee, FL
[2]Division of Earth and Ocean Sciences, Duke University, Durham, NC
[3]Center for Ocean-Atmospheric Prediction Studies, Florida State University, Tallahassee, FL
[4]Integrative Oceanography Division, Scripps Institution of Oceanography, La Jolla, CA

* Corresponding Author: Sven A Kranz (skranz@fsu.edu)

Keywords: Gross Primary Production, Long Term Ecological Research, Equilibrium Inlet Mass spectrometry, Carbon Export, Net Community Production,

Index Terms:

4227 Diel, seasonal, and annual cycles, 0460 Marine systems, 0414 Biogeochemical cycles, processes, and modeling, 4806 Carbon cycling, 4820 Gases

Abstract

Upwelling of nutrient rich waters along continental shelves generates highly productive marine ecosystems affecting planktonic communities from coastal to offshore domains. Methods to constrain pelagic productivity are often based on different physiological or ecosystem processes, hence describe different biogeochemically important processes. Here, we present a multi-method process-oriented investigation of diverse productivity measures in the California Current Ecosystem (CCE) Long-Term Ecological Research study region, a complex physical environment. The data are from seven multi-day deployments over two field expeditions (spring 2016 and summer 2017) and cover a transition region from high to low productivity. Employing a Lagrangian study design, we aimed to follow the water parcels over several days, comparing 24 h in-situ measurements (^{14}C and $^{15}NO_3$, uptake, sediment trap export, dilution estimates of phytoplankton growth and microzooplankton grazing) with high-resolution productivity measurements by Fast Repetition Rate Fluorometry (FRRF) and Equilibrium Inlet Mass Spectrometry (EIMS). Our results show the importance of accounting for temporal and fine spatial scale variability when estimating ecosystem production. FRRF and EIMS measurements resolved diel patterns in gross primary and net community production. Diel productivity changes agreed well with comparable more traditional measurements. While differences in productivity metrics calculated over different time intervals were considerable, as those methods rely on different base assumptions, our data can be used to explain ecosystem processes which would otherwise have gone unnoticed. The processes resolved from this method comparison can help to further our understanding of the coupling and decoupling of surface productivity and potential carbon burial in coastal and offshore ecosystems.

Plain Language Summary

The California Current Ecosystem (CCE) is a site of coastal upwelling and is among the most productive ecosystems in the world oceans, supporting fisheries of much of the western United States, while playing a vital role in the economy of coastal communities. Accurately assessing marine productivity in such regions is important in order to understand the flux of carbon through the food web and the ocean's ability to sequester carbon dioxide. Productivity assessments are, however, often based on different methodologies relying on distinct cellular or ecosystem assumptions. Each individual method can thus be misleading if its assumptions are not met, while any single method is likely to fall short in terms of explaining ecosystem

dynamics. Here, we present a multi-method process-oriented investigation of diverse productivity methods in the CCE Long-Term Ecological Research study region. Traditional 24h in-situ incubation methods were compared to high temporal resolution measurements using advanced optical and mass spectrometric methods. The productivity rates and ecosystem processes resolved presented here can help to further our understanding of the linkages between photosynthesis and respiration or carbon production and sequestration. This approach can also help to improve productivity assessments in complex ecosystems and to resolve the time-scales of these processes.

1. Introduction

Upwelling plays a key role in driving marine primary production along the eastern continental margins of the world's oceans (Chavez & Messie, 2009; Dugdale, 1972; Dunne et al., 2007; Kudela et al., 2008; Longhurst et al., 1995; Muller-Karger et al., 2005). Upwelled water rich in inorganic nutrients can support intense phytoplankton blooms, typically dominated by large diatoms that efficiently transfer newly produced biomass to higher trophic levels and into the mesopelagic via sinking (Kumar et al., 1995; Michaels & Silver, 1988; Stock & Dunne, 2010; Thunell et al., 2007). Lateral transport also provides a significant flux of upwelled nutrients and coastal planktonic communities to the offshore domain (Nagai et al., 2015; Plattner et al., 2005), resulting in complicated spatial and temporal connectivity between physical forcing, *in situ* community composition and regional biogeochemistry.

While remote sensing techniques can reasonably quantify phytoplankton standing stocks (O'Reilly et al., 1998; Saba et al., 2011), primary production (Behrenfeld & Falkowski, 1997; Kahru et al., 2015), and even community composition (Pan et al., 2011; Uitz et al., 2015), over broad temporal and spatial scales, fine-scale and subsurface features remain challenging to resolve from satellites. By the same token, shipboard incubation techniques allow more accurate measurements throughout the photic zone, but are time-intensive and limited for resolving patterns in highly heterogenous regions. In addition, shipboard methods with different assumptions, caveats and spatiotemporal integration can be challenging to compare among cruises and regions. In this regard, multi-method approaches for assessing productivity have proven useful for understanding the nuances of processes that shape production responses to

varying environmental conditions and their relationships (e.g. Hamme et al., 2012; Quay et al., 2010; Robinson et al., 2009; Teeter et al., 2018).

Here, we take such a multi-method approach to reveal commonalities and complications among several ecosystem production techniques applied to heterogeneous environmental settings in the California Current Ecosystem (CCE) from coastal upwelling to the oligotrophic open ocean. We especially want to emphasize that novel productivity assessment techniques can reveal high temporal and spatial resolution of marine productivity which can in turn prove useful in characterizing ecosystem productivity patterns. In the following section, we first touch briefly on the various definitions and methods for assessing primary productivity and their issues. We then describe process-oriented investigations on two field expeditions (spring 2016 and summer 2017; Fig. 1) in the CCE-LTER (Long Term Ecological Research) study region off of southern California on which we compared traditional *in situ* measurements (^{14}C, $^{15}NO_3^-$, dilution-based growth rates, and sediment traps) for assessing net primary production (NPP), new production (NP) and export production to high-resolution production measurements of net carbon production (NCP), O_2:Ar-based gross primary production (GPP) and FRRF-based photophysiological measurements of GPP. Two novel aspects of the study are highlighted. First, we utilized a Lagrangian approach, tracking water parcels for several days, which allowed us to follow the evolution of production processes during advective transport and to measure some aspects of diel variability. Second, we field-tested and compared results for a new approach, described in detail in a companion paper (Wang et al., submitted), that uses O_2/Ar to resolve temporal and spatial patterns of NCP in a highly dynamic region. To our knowledge, this study comprises the first in-depth analysis of so many different production assessments in a highly dynamic coastal setting. While some differences are noted, as expected from the different processes measured, results from temporally resolved production approaches are surprisingly consistent with traditional production measurements, indicating that such approaches could provide important new insights into the production dynamics of physically complex systems.

2. Overview of Production Definitions and Measurement Approaches

The many different techniques for assessing ocean production can be reasonably grouped in a few broadly defined measurement categories. Gross Primary Production (GPP) is the rate of organic carbon production by autotrophs. Net Primary Production (NPP) refers to GPP minus the

respiration performed by the autotrophs themselves. NPP thus accounts for both growth and metabolic loss processes that lead to phytoplankton biomass production. The term New Production (NP) refers to the portion of phytoplankton production based on the uptake of "new" nitrogen (N) that enters the euphotic zone from external sources. NP sources include upwelled NO_3^-, believed to be the dominant source of "new" nitrogen in the CCE, as well as nitrogen delivered by atmospheric deposition, riverine input or nitrogen fixation. Export Production measures the rate of carbon exported out of the euphotic zone where primary production occurs, which is generally defined as the depth of penetration of 1% or 0.1% surface irradiance. Net Community Production" (NCP), sometimes also called net ecosystem production, is defined as GPP minus the respiration of all organisms in the ecosystem. As most production is eventually respired at the community level, NCP rates need to be constrained by depth or time boundaries. When integrated over appropriate spatial and temporal scales and converted to common units, NCP, NP and export production should be in balance, representing the total amount of carbon or nitrogen that can be exported from the euphotic zone by the biological carbon pump without depleting biomass (Eppley & Peterson, 1979).

One of the most common methods for estimating primary production is the incorporation of ^{14}C-labelled bicarbonate into particulate organic carbon (Steemann Nielsen, 1952). Although this highly sensitive method has been a standard for aquatic production studies for decades, interpretation is still highly debated (Marra, 2009; Peterson, 1980). Measurements conducted over a relatively short time approximate GPP, but longer incubations have increasing losses to respiration. Experiment conducted over the full 24-h photocycle are thought to approach to NPP, but should be underestimates because the respiratory losses include contributions from heterotrophs that had consumed labelled C, in addition to respiration from autotrophs. Interpretations are further complicated by starting incubations at different times of day, requiring different weighting for uptake and respiration. Additionally, production can be significantly underestimated when incorporation of ^{14}C into Dissolved Organic Carbon (DOC) is unmeasured (Laws et al., 2000; Myklestad, 2000; Teira et al., 2001). NPP can also be assessed by the seawater dilution method, where serial dilution is used to decouple growth and grazing processes, allowing separate instantaneous rate estimates for phytoplankton growth and microzooplankton grazing (Landry & Hassett, 1982). When carbon-based biomass estimates for phytoplankton is combined with dilution-based daily rates, the calculated NPP result is the daily

net carbon biomass produced by phytoplankton absent losses that are a consequence of grazing (Barron et al., 2014; Landry et al., 2000).

The uptake and incorporation of $^{15}NO_3^-$ into phytoplankton cells can also be used to estimate phytoplankton production derived from that nitrogen source (Dugdale & Goering, 1967). The $^{15}N\text{-}NO_3^-$ method is thought to reduce the impact of internal elemental turnover, a process much enhanced in the cellular carbon pool compared to cellular nitrogen. The measurement is based on the enrichment of ^{15}N in cellular particulate organic nitrogen (PON) over the incubation period and is defined as NP, under the assumption that nitrate is not regenerated from ammonium in the euphotic zone. This method can, however, be impacted by processes such as ammonification or nitrification in surface waters (Yool et al., 2007) which lead to under- or overestimates of NP. In addition, luxury NO_3^- uptake (Painter et al., 2007) and release of previously fixed ^{15}N as DON can also affect results of the ^{15}N method (Bronk et al., 1994; Collos, 1998).

NCP, the balance between photosynthesis and community respiration, can be measured from the oxygen budget of the ocean mixed layer. Because of the similar physical properties of O_2 and Ar, NCP measurements based on the O_2/Ar method are mostly immune to mixed-layer physical effects (e.g. solubility, gas exchange) on O_2 budgets over timescales of days to weeks. However, coastal upwelling systems complicate the assumptions for this method (Teeter et al., 2018) since such coastal water parcels exhibit a larger magnitude of short-term variations in productivity and are subject to strong vertical fluxes that can alter surface O_2/Ar. Nonetheless, recent work has shown that NCP can be applied on shorter timescales (Hamme et al., 2012) if the measurements are conducted in a Lagrangian reference framework. Shortcomings of and improvements on this method, which is used in our CCE method comparison, are discussed in detail in a companion paper by (Wang et al., submitted).

Short-term measurements by the O_2/Ar method can also be used to estimate GPP if done in the same Lagrangian-tracked water mass during the day (production + respiration) and night (respiration) and assuming that nighttime respiration rate applies to the day. GGP is more rigorously determined using isotopically labelled water ($H_2{}^{18}O$) (Goldman et al., 2015) or oxygen ($^{18}O_2$) (Kranz et al., 2010) or from the natural isotopic composition of oxygen by the $^{17}\Delta O_2$ triple O_2 isotope method (Luz & Barkan, 2005). However, these methods do not allow for high-resolution spatiotemporal sampling and were not used here. Alternatively, the conversion

of sunlight into a biological redox potential in phytoplankton (i.e. electron generation at photosystem II; PSII) can be assessed indirectly by variable fluorometry to provide another nonintrusive PSII photochemical approach for estimating GPP at fine spatiotemporal scales. Using the Single Turnover Method (STM) (Falkowski & Kolber, 1993; Kolber & Falkowski, 1993; Moore et al., 2006; Oxborough et al., 2012; Suggett et al., 2001) cellular energy allocation between photochemical (energy generation and fixation of inorganic nutrients) and non-photochemical (energy dissipation if excitation exceeds photochemical quenching) processes can be quantified. However, the interpretation of the fluorescence signal is affected by environmental conditions such as nutrient limitation, signal quenching under high-light intensities, as well as other methodological sensitivities. Recent studies have recommended multiple improvements to reduce uncertainties of the STM method (Boatman et al., 2019; Oxborough et al., 2012; Schuback & Tortell, 2019), some of which we have applied in the present study. Most notably, however, O_2:Ar-based NCP and GPP and variable fluorescence-based GPP approaches are incubation-independent production measurements free from "bottle effects" and amenable to flow-through applications that enable high spatiotemporal resolution sampling.

3. Material and Methods

3.1 Cruise Background

Production measurements were made during quasi-Lagrangian experiments conducted on two Process cruises of the CCE LTER Program (Figure 1). The first cruise (RAPID CCE-LTER cruise P1604, 19 April to 12 May 201, *R/V Sikuliaq*) investigated ecosystem responses during the 2015-2016 El Niño (Jacox et al., 2016) and had a wide geographic focus ranging from coastal upwelling to oligotrophic offshore conditions (Morrow et al., 2018; Nickels & Ohman, 2018). The second cruise (P1706, 1 June to 2 July 2017, *R/V Roger Revelle*) followed community and biogeochemical changes along a mesoscale filament transporting coastal waters to the offshore domain. Experiments were thus conducted in a gradient ranging from newly upwelled water to aged waters with a declining phytoplankton bloom. During both cruises, 3-4 quasi-Lagrangian experiments (hereafter 'cycles') were conducted, yielding 7 total cycles. Cycles averaged ~3.5 days during which the cruise track followed a satellite-tracked Lagrangian drifter (Figure 1). Deployment areas were first surveyed with a Moving Vessel Profiler (MVP) (Ohman et al., 2012) to ensure that they represented a cohesive water parcel free of strong frontal gradients. The

cycle was then initiated by deploying a sediment trap array followed by an array used for in situ incubations (Landry et al., 2012; Stukel et al., 2013). Both arrays had a 3×1-m holey sock drogue centered at 15-m depth in the surface mixed layer and followed similar drift paths during the cycles.

3.2. Chlorophyll-a and Inorganic Nutrients

During each day of a cycle, samples for chlorophyll and nutrients were taken with CTD Niskin bottles at 8 depths spanning the photic zone. Chlorophyll-*a* was extracted following Strickland and Parsons (1972). A more detailed description of sample analysis can be found in the supplemental materials (S-M 1). Nutrient samples were filtered using a 0.1µm Acropak filter prior to freezing for shore-based analysis. Dissolved inorganic nutrients (nitrate, nitrite, silicate, phosphate and ammonium) were analyzed using an automated flow injection autoanalyzer on a Lachat Instruments QuikChem 8000 (Gordon et al., 1992). The precision of these measurements was ± 5%, and the detection levels for nitrate + nitrite, nitrite, ammonium, phosphate and silicate were 0.2, 0.1, 0.1, 0.1 and 1.0 µM, respectively.

3.3. Bottle incubations: ^{14}C Net Primary Production (NPP_{14C}) and $^{15}NO_3^-$ New Production (NP)

^{14}C Net Primary Production (NPP_{14C}) and $^{15}NO_3^-$based New Production (NP) were quantified from *in situ* incubations for each day of the cycles at 6 depths spanning the euphotic zone. Niskin bottle samples were gently transferred to polycarbonate incubation bottles (triplicate 250-mL bottles plus a dark bottle for NPP_{14C} and a single 1-L bottle for NP) using silicon tubing. Samples were then spiked with $H^{14}CO_3^-$ (NPP_{14C}) or $K^{15}NO_3^-$ (NP) and incubated for 24 h in mesh bags hung below the drift array. Incubations were started and terminated at ~04:00 local time. NPP_{14C} samples were then filtered onto GF/F filters, acidified for 24 h, placed in scintillation cocktail, and subsequently counted using a liquid scintillation counter (details in (Morrow et al., 2018). NP samples were filtered onto GF/F filters and frozen at sea. On land, they were acidified, dried, and analyzed by isotope ratio mass spectrometry at the UC Davis Analytical Facility. Nitrate uptake was calculated following (Dugdale & Wilkerson, 1986) with a slight modification similar to ρ_{is} in (Kanda et al., 2003) when the nitrate spike was >10% of

ambient nitrate (Stukel et al., 2016). On the P1706 cruise, NPP_{14C} samples were lost and NPP_{14C} was estimated using an algorithm fitted to CCE NPP_{14C} data, as described below.

3.4. Net Production Estimates based on Chlorophyll, Light and Nutrients

For the P1706 cruise, we estimated NPP rates from ambient light, nutrients, and Chl *a* as described by (Stukel et al., 2019a). The initial algorithm was developed using irradiance to predict Chl *a* specific production (Morrow et al., 2018) and then adapted for general use in the CCE. The algorithm was parameterized from data collected on seven previous CCE-LTER process cruises for which ^{14}CPP data were available. P1706 NPP was subsequently calculated as:

$$\frac{NP}{Chl} = V_{0m} \cdot \left(1 - \mathrm{e}^{(-\alpha \cdot PAR/V_{0m})}\right) \cdot \frac{NH_4}{NH_4 + K_S} \qquad \text{(Eq. 1)}$$

where NP/Chl is the chlorophyll-specific primary production in units of mg C d^{-1} (mg Chl)$^{-1}$, PAR is average daily photosynthetically active radiation (units of µmol photons m^{-2} s^{-1}) within the mixed layer, $\left(1 - \exp(-\alpha \cdot PAR/V_{0m})\right)$ describes the light saturation and inhibition term with V_{0m} = 66.5 mg C d^{-1} (mg Chl)$^{-1}$ and α = 1.5; and $\frac{NH_4}{NH_4+K_S}$ describes the ammonium-limitation kinetics with K_S = 0.025 µmol L^{-1}. Uncertainties in the algorithm were propagated through all subsequent equations following (Stukel et al., 2019a) When averaged over the duration of a cycle, propagated errors in mixed layer NPP were ± 30 – 40% at the 95% confidence limit.

3.5 Net Phytoplankton Production from Dilution Experiments ($NPP_{G:G}$)

To calculate phytoplankton intrinsic growth rates and microzooplankton grazing rates, dilution experiments were prepared following the two-treatment dilution approach (Landry et al., 2008; Landry et al., 2011b; Stukel et al., 2012). Each experiment consisted of water collected at 6 depths spanning the euphotic zone (i.e. "array depths") in pre-dawn CTD casts (02:00 local). At each depth, two 2.7 L polycarbonate bottles were filled with either unfiltered seawater (i.e. 100% whole seawater) or a mixture of 33% whole seawater and 67% 0.1-µm filtered seawater. Samples were incubated in situ on the drifter array for 24 h along with the NPP_{14C} and NP experiments. Net growth rates in each bottle were determined from changes in fluorometrically-measured Chl a and used to quantify gross growth rates (µ) and mortality due to protistan grazing

(m). Carbon to Chl *a* ratios (C:Chl) were determined using the approach of Li et al. (2010), based on microscopy-derived estimates of phytoplankton biomass in the CCE region. C:Chl was multiplied by Chl to determine initial carbon biomass (B_0), and & phytoplankton production was calculated as $NPP_{G:G} = \mu\, B_0\, e^{\mu - m}/(\mu - m)$, following Landry et al. (2016).

3.6. Net and Gross Community Production from O_2/Ar Measurements (NCP; $GPP_{O2/Ar}$)

Continuous samples of dissolved O_2/Ar were taken from the ship's underway seawater system. O_2/Ar gas ratios were measured with a Pfeiffer QMC 200 mass spectrometer equipped with an equilibration inlet (EIMS) (Cassar et al., 2009). Temperature and oxygen concentrations were measured using Aandera temperature sensors (model 3835) and oxygen optodes. The signal was filtered to within an 8 km distance between the ship and the drifter (e.g. removing values during plankton net tows when the ship was far from the drifter location), and calibration and maintenance times were also removed. Net rates of community production (NCP) from O_2/Ar measurements reflect oxygen production by photoautotrophs, respiration by photo- and heterotrophs and corrections for physical gas exchange processes. NCP rates are calculated for the mixed layer depth (MLD) assuming no advective fluxes of O_2/Ar from neighboring water parcels and represent processes occurring over the residence time of O_2 assuming a steady state system:

$$NCP_{prior} = k \cdot \Delta(O_2/Ar)[O_2]_{sol}\rho \qquad \text{(Eq. 2)}$$

NCP_{prior} estimates the time-averaged NCP based on wind speed history, MLD, and the observed biological oxygen signal, where k is the time-weighted piston velocity (see Reuer et al., 2007) incorporating the wind speed history and MLD. $[O_2]_{sol}$ is the mixed layer oxygen solubility, and ρ is the average density of the mixed layer. $\Delta(O_2/Ar)$ is the biological oxygen signal defined by $\Delta(O_2/Ar) = \frac{(O_2/Ar)}{(O_2/Ar)_{cal}} - 1$. Due to our Lagrangian study design, we were able to measure short-term changes in mixed layer $\Delta(O_2/Ar)$ in real time ("instantaneous changes") and thereby estimate NCP over shorter timescales than the residence time of mixed layer O_2 (see Hamme et al., 2012; Teeter et al., 2018; Wang et al., submitted).

$$NCP_{inst} = z\frac{\Delta(\Delta(O_2/Ar))}{\Delta t}[O_2]_{sol}\rho + \bar{k}(\Delta O_2/Ar)[O_2]_{sol}\rho \qquad \text{(Eq. 3)}$$

where z denotes MLD and $\bar{k}$ represents the instantaneous gas exchange coefficient averaged over the preceding hour (i.e. Δt). Using community respiration measured during the night, $NCP_{(inst,night)}$ & assuming similar day and night respiration, GPP can be estimated as:

$$GPP_{NCP} = NCP_{inst,day} - NCP_{inst,night} \quad \text{(Eq. 4)}$$

3.7. Estimating Mixed-Layer GPP using FRRF

In addition to the O_2/Ar method, we also estimated GPP independently on the P1706 cruise based on the photo-physiology of the mixed-layer phytoplankton community measured by FRRF. Shipboard measurements were made using a bench-top FastAct 2+ Fast TRAKA instrument (Chelsea, UK) plumbed into the ship's running seawater system. Photosynthesis versus irradiance (P vs. I) curves were run continuously on a ~45 min sampling interval. Using a modified version of the absorbance algorithm following Oxborough et al. (2012), volume-based productivity rates (i.e. mol electrons $(RCII)^{-1}$ m^{-3} d^{-1}) are calculated as:

$$JV_{PSII,abs} = \Phi_{RCII} \cdot F_o' \cdot K_a \cdot E \cdot 8.64 \times 10^{-8} \quad \text{(Eq. 5)}$$

where $F_o' = (F_m \cdot F_0)/(F_m - F_0) \cdot (F_q'/F_m)$. $K_a = 11800$ m^{-1} is an instrument-specific calibration factor, E = irradiance (µmol photons m^{-2} s^{-1}), the factor 8.64×10^{-8} converts µmol photons m^{-2} s^{-1} to mol photons m^{-2} d^{-1} and kg/m^{-3} to mg/m^{-3}. The parameter Φ_{RCII} (mol e^- mol $photon^{-1}$) has a constant value of 1, representing one electron transferred from P680 to quinone A (Q_A) for each photon absorbed and delivered a reaction center (RCII) (Kolber & Falkowski, 1993). RCII was estimated as:

$$RCII = K_a \cdot {}^{F_0}/_{\sigma_{PSII}} \quad \text{(Eq. 6)}$$

where F_0 is dark-adapted base fluorescence and σ_{PSII} is the absorption cross-section area of the photosystem. As the RCII estimate might be biased by base fluorescence quenching during daytime, JV_{PSII} was corrected using an average RCII estimate from nighttime measurements (01:00 – 05:00 local). JV_{PSII} (mol electrons m^{-3} d^{-1}) was converted to carbon units using the conversion factor Φe:c (Schuback & Tortell, 2019):

$$\Phi_{e:C}/\,\eta_{RCII} = 486 \cdot NPQ_{NSV} + 1854 \quad \text{(Eq. 7)}$$

where $\Phi_{e:C}$ is the electron generation to carbon fixation ratio, η_{RCII} is the RCII to Chl-*a* ratio and NPQ_{NSV} is the normalized Stern-Volmer non-photochemical quenching coefficient. For simplicity, we used a literature value of 0.003 for η_{RCII} (Lawrenz et al., 2013) but recommend that η_{RCII} be measured directly on future cruises to avoid biasing estimates of $\Phi_{e:C}$. More detailed descriptions of the measured and calculated parameters and additional information for the production estimates using FRRF are provided in the supplemental material (Table S1).

To calculate mixed-layer GPP from FRRF measurements, we used the *in situ* light attenuation from the CTD profile around noon to calculate the light field in the mixed layer over the diurnal cycle. The time-varying *in situ* light field was modeled using the empirical transmission-light attenuation relationship and surface photosynthetically active radiation (PAR) measured by the ship's meteorological system. Photosynthesis vs. irradiance relationships were determined by fitting the productivity rate estimates from the FRRF versus the irradiance from the FRRF light curves using the Platt et al. (1980) definition:

$$Productivity = Ps \times [1 - e^{\frac{-\alpha \times E}{Ps}}] \times e^{\frac{-\beta \times E}{Ps}} \qquad \text{(Eq. 8)}$$

where Ps equals the maximum photosynthesis, E equals is the irradiance (PAR), α is the initial slope of photosynthesis under low irradiance and β is the slope under high/stressful irradiance. Additional methods on photophysiology including a table with the nomenclature is available in the supplemental material (methods S1 and Table S1).

3.8. Sediment Trap Deployments

We deployed VERTEX-style surface-tethered drifting sediment traps (Knauer et al., 1979) near the base of the euphotic zone. Trap crosspieces holding 12 acrylic tubes with an 8:1 aspect ratio, topped with baffles constructed of smaller beveled tubes, were deployed on a line with surface floats and a holey-sock drogue centered at 15-m depth. Tubes were deployed with a saltwater brine of filtered seawater and 0.4% formaldehyde. After recovery, overlying seawater was removed by gentle suction, and samples were analyzed under a dissecting microscope to remove mesozooplankton 'swimmers'. Samples were then split on a Folsom splitter, filtered onto pre-combusted GF/F filters, acidified and analyzed for C, N, and isotopes on an isotope ratio mass spectrometer at the UC Davis Stable Isotope Facility. Previous comparisons with independent export flux estimates made using ^{238}U-^{234}Th disequilibrium approaches have shown

no substantial over- or under-collection biases for our sediment trap configuration in the CCE (Stukel et al., 2019). For additional deployment and processing details, see Stukel et al. (2019b).

3.9. Statistics

For all cycle data, variability was quantified as the standard errors of the means using the available 24-hour integrated data. Since intra-cycle variability was a combination of measurement uncertainty and ecosystem variability, standard parametric statistics were not applicable. Throughout this manuscript, we present vertically integrated rates throughout the mixed layer, unless otherwise stated. For bottle samples, we used trapezoidal integration. For the NPP_{14C} algorithm used for the P1706 cruise, uncertainties in parameter estimates were propagated through all equations.

4. Results

4.1. General Features of the Two Cruises

Four different regions were sampled during the P1604 cruise (Figure 1): the offshore stratified region (P1604-C1), the core of the California Current (P1604-C2), offshore of the coastal boundary in the wind stress curl upwelling domain (P1604-C3), and the coastal boundary upwelling region (P1604-C4). Over the course of 4 cycles on P1706, we followed upwelled waters from nearshore to offshore. P1706-C1 was located in freshly upwelled waters; P1706-C2 started ~77 km NW of the end of P1706-C1 in partially aged upwelled waters; and P1706-C3 began ~140 km southwest of the start of P1706-C2 in post-bloom waters. Post-cruise analysis indicated that P1706-C3 was not part of the main filament and contained water characteristic of the California Current, likely advected from the North. P1706-C4 was a continuation of P1706-C2 initiated about 26 km northeast of the start of P1706-C3 (Figure 1). Average mixed-layer depth, temperature, Chl *a*, nutrient concentrations are given in Table S2 for all cycles. Full data are available in the CCE-LTER database: https://oceaninformatics.ucsd.edu/datazoo/catalogs/ccelter/datasets?fc= 11:29820&ps =1:0_2:0_3:0_9:0_11:0.

4.2. Phytoplankton Production

4.2.1. ^{14}C Primary Production

^{14}C-derived estimates of NPP are from field incubations conducted during P1604 and from a general algorithm based on CCE field incubations for P1706 (Stukel et al. 2019). Both are defined as NPP_{14C} and treated the same

NPP_{14C} decreased slightly between successive days during P1604-C2 (22, 17 and 14 mmol C m^{-2} d^{-1}), increased daily during P1604-C3 (36, 45 and 64 mmol C m^{-2} d^{-1}), and had the highest rates (150, 103 and 113 mmol C m^{-2} d^{-1}) during P1604-C4 (Fig. 3, Table S4). A strong gradient of decreasing NPP_{14C} with distance from shore is therefore evident in the P1604 data.

NPP_{14C} for P1706 showed a wider range of results but a similar decrease from nearshore to offshore (Fig. 4, Table S4). In freshly upwelled waters during P1706-C1, production tripled from 220 mmol C m^{-2} d^{-1} for day 1 (D1) to 718 and 596 mmol C m^{-2} d^{-1} for D2 and D3, respectively. In P1706-C4 offshore waters, average NPP_{14C} was 30-fold lower (13 and 19 mmol C m^{-2} d^{-1} for D1 and D2, respectively). Between these extremes, NPP_{14C} varied from ~250 to 300 mmol C m^{-2} d^{-1} during P1706-C2 and decreased from ~90 to 48 mmol C m^{-2} d^{-1} from D1 to D3 during P1706-C3.

4.2.2. $NPP_{G/G}$ from Dilution Growth and Grazing Rates

$NPP_{G/G}$ estimates closely follow the magnitudes and trends observed for NPP_{14C} (Table 1). Mean rates are higher for P1604-C3 compared to C2 (48.4 ± 8.4 vs 17.7 ± 4.5 mmol C m^{-2} d^{-1}) and decrease even further to 9.4 mmol C m^{-2} d^{-1} during P1604-C1. For P1604-C2, day-to-day $NPP_{G/G}$ variability (44, 24 and 36 mmol C m^{-2} d^{-1} for D1-D3, respectively), is similar to that of NP and NPP measurements. During P1604-C3, $NPP_{G/G}$ increased from 49 to 76 mmol C m^{-2} d^{-1} over the 3-day occupation, similar to the increase in independently measured NPP_{14C}. While no $NPP_{G/G}$ data were obtained for the nearshore P1604-C4, the high rates were found in the freshly upwelled waters of P1706-C1 (511 ± 150 mmol C m^{-2} d^{-1}; range 252 to 588 mmol C m^{-2} d^{-1}). Over subsequent P1706 experiments, $NPP_{G/G}$ decreased each day along the upwelling filament, averaging 270 ± 44, 76 ± 39 and 22 ± 6 mmol C m^{-2} d^{-1} for cycles 2 to 4, respectively.

3.2.3: New production ($^{15}NO_3$ uptake)

Mixed-layer integrated rates of nitrate-based new production (NP) are given in Table 1 as carbon equivalents using a N:C conversion of 6.625. For P1604, mean NP rates of 11 ± 3 mmol C m^{-2} d^{-1} during offshore cycle 2 increased to 24 ± 8 and 23 ± 6 mmol C m^{-2} d^{-1}, respectively, during cycles 3 and 4. For P1706, NP was highest (157 ± 19 mmol C m^{-2} d^{-1}) in C1 upwelled waters, and declined progressively during offshore filament transport. NP averaged 101 ± 44 mmol C m^{-2} d^{-1} during P1706-C2, but decreased by 75% from days D1 and D2 to D3 (Table S4). Further offshore, NP decreased to 29 ± 18 and 5 ± 0.1 mmol C m^{-2} d^{-1} during C3 and C4 , respectively. *f*-ratios (the ratio of new production to total production, estimated as NP/NPP_{14C}) varied from 0.2 to 0.7 over all experiments but lacked a consistent onshore-offshore trend (Table 1).

3.2.4: Net community Production (NCP_{prior})

Conventional O_2/Ar-NCP estimates in complex systems such as the CCE are challenging to interpret. Our companion paper (Wang et al., submitted) discusses these shortcomings along with method improvements used to estimate NCP more reliably in the present field campaigns. Here, we use these new insights in discussing the traditional NCP analysis (NCP_{prior}) and a real-time NCP (NCP_{inst}), which integrate O_2/Ar signals over different time scales. The O_2 residence time, as determined by wind-speed reanalysis and mixed layer depth was between 6.6 and 15.6 days for P1604 and between 2.6 and 9.0 days for P1706 (Wang et al., submitted). During both cruises, the heterogenous nature of NCP in the CCE-LTER region is indicated by significant short- and long-term trends in NCP_{prior} (Figs. 3, 4).

NCP_{prior} was steady and low during P1604-C2 and highest during P1694-C4 (5.5 ± 0.3 and 39.5 ± 4.0 mmol C m^{-2} d^{-1}, respectively; Table 1). Although the water mass appeared well equilibrated with the atmosphere during P1604-C3, NCP_{prior} changed from slightly net heterotrophic at the beginning of the cycle (-10.7 mmol C m^{-2} d^{-1}) to slightly net autotrophic (8.6 mmol C m^{-2} d^{-1}) at the end, averaging -0.3 ± 5.6 mmol C m^{-2} d^{-1}. NCP_{prior} showed clear diurnal amplitudes during P1604-C2 and C4, with increasing rates during daylight and decreasing rates at night (Fig. 3). The diurnal amplitude was, however, less pronounced during P1604-C3.

4.2.5. Real-time Analysis of NCP (NCP_{inst})

Real-time analysis of NCP data (NCP_{inst}) accounts mainly for O_2/Ar change over the previous 1 hour, including the instantaneous gas exchange coefficients. The system was net

autotrophic for P1604-C2 and C4, decreasing from 9.7 to 1.1 mmol C m^{-2} d^{-1} over the duration of C2 (Table S4) and subsequently increasing to 16.4 ± 4.0 mmol C m^{-2} d^{-1} for C4 (Tables 2 and S4). NCP_{inst} indicates a slightly net heterotrophic system (-0.1± 1.2 mmol C m^{-2} d^{-1}) during P1604-C3.

NCP_{inst} estimates were net autotrophic for P1706-C1 (77.8 ± 0.5 mmol C m^{-2} d^{-1}) and net heterotrophic for P1706-C2 (-14.3 ± 11.3 mmol C m^{-2} d^{-1}). For cycles 3 and 4, the signals were strongly affected by ship movements through other waters mixed in with the relatively narrow filament. Consequently, we view these NCP_{RT} estimates as unreliable and do not discuss them further.

4.2.6 Gross Primary Production based on NCP ($GPP_{O2/Ar}$)

$GPP_{O2/Ar}$ averaged 42 ± 9 and ~130 mmol C m^{-2} d^{-1} for P1604-C2 and C3, respectively. No error determination could be made for C3 as the respiration measurements during days 1 and 2 were positive values when the ship moved through different water masses; hence, only day 3 date could be used for this cycle. High $GPP_{O2/Ar}$ rates were estimated for nearshore cycles P1604-C4 (4348 ± 171 mmol C m^{-2} d^{-1}) and P1706-C1 (1082 ± 134 mmol C m^{-2} d^{-1}). For P1706-C2, estimated GPP declined to 401± 52 mmol C m^{-2} d^{-1}. As noted above, estimates for P1706-C3 and C4 were compromised by ship movements through mixed waters.

4.2.7. GPP_{FRRF} Estimates

No FRRF measurements were conducted during P1604. For P1706, mean GPP_{FRRF} estimates declined progressively following along onshore-to-offshore filament transport of upwelled water from 934 ± 207 to 630 ± 122 µg C m^{-2} d^{-1} for C1 and C2, respectively, to 115 ± 25 and 35 ± 1 µg C m^{-2} d^{-1}, for C3 and C4 (Fig. 4F, Table 1). For P1706-C1, diurnally averaged GPP increased with time spent in the water mass (519 to 1148 µg C m^{-2} d^{-1} for D1 to D3; Table S4). For other P1706 cycles, GPP was relatively constant or decreased slightly (Table S4). As shown in Fig. 4, GPP rates showed a distinct diurnal periodicity with notably higher rates during the noon/afternoon hours. Spikes during P1706-C1 and C2 are most associated with occasional net tows when the ship briefly left the drift array and entered water parcels with higher surface Chl a.

4.3. Photophysiology and Light Acclimatization

Changes in production are not only associated with light intensity, nutrient availability or phytoplankton abundance. Light acclimatization can play a large role in the ability of phytoplankton to utilize available light efficiently or dissipate excess light. As such, we evaluated photophysiology and light absorption characteristics for all P1706 cycles (Figs. S1). The maximum quantum yield (F_v/F_m) of the dark-adapted phytoplankton community for P1706-C1 was around 0.48 to 0.5 during nighttime and morning hours but dipped to ~0.4 at the end of the photoperiod of D2 and D3. Values of ~0.5 are the maximum measurable in non-stressed cells using single turnover measurements with our FRRF instrument. For P1706-C2, Fv/Fm was lower (0.39-0.42) during night and morning hours, but also showed a relative decline towards the end of each photoperiod. Fv/Fm increased steadily from 0.4 to ~0.49 during P1706-C3 but was relatively constant (~0.45) for P1706-C4. Both of these cycles (C3 and C4) were dominated by smaller phytoplankton, mainly cyanobacteria, and neither displayed the distinct diel decreases in Fv/Fm as seen un C1 and C2. Generally, lower overall Fv/Fm values indicate conditions that negatively affect photosystem function in the phytoplankton community, such as iron (Fe) limitation. Iron limitation is yet not only associated with a loss in quantum yield efficiency but more importantly the optical absorption cross section of the photosystem (σ) the area of chlorophyll pigments available to absorb light around a reaction center, and the reoxidation rate of the Quinone A in PSII ($1/\tau$) (Kolber et al., 1994). The absorption cross sectional area of PSII (σ), did not show a diel pattern, yet, σ was enhanced during C2 (6 nm^2 $PSII^{-1}$) compared to C1 (4 - 5 nm^2 $PSII^{-1}$). For C3, σ was 6 nm^2 $PSII^{-1}$ while in C4 the absorption cross sectional area of PSII was 5.5 nm^2 $PSII^{-1}$. $1/\tau$ decreased throughout the light phase and increased during the dark period. This pattern was well defined in C1 and C2, dampened in C3 and non-existent in C4. Compared to C1, $1/\tau$ increased in our C2 measurements, yet it should have decreased under Fe limitation which was likely driven by changes in the phytoplankton community. Potential Fe limitation during P1706-C2, was independently determined based on diagnostic nutrient ratios (Si:N and Fe:N; Fulten and Barbeau, pers. comm.) and Fe amendment experiments (K. Forsch and K. Barbeau, pers. comm.). In addition, enhanced NPQ rates (data not shown) were measured in C2, demonstrating an enhanced energy dissipation through non-photochemical processes in Fe limited cells under ambient light. The enhanced NPQ did affect our productivity rate estimate, as NPQ values are used to calculate the electron to carbon ratio (see Eq. 7; Schuback et al., 2018). Parameters derived from the fluorescence induction curves (α, P_{max}) showed some

variability within and between cycles. Maximum photosynthetic electron transport (P_{max}) increased towards the ends of each photoperiod in C1 and C2, but was relatively constant for C3 and C4 (Fig. S1). α did not show diel changes, yet, values for C1 and C2 were significantly lower compared to C3 and C4. The light saturation point (Ek) (averages, including light and dark phase, were 427 ± 106 for C1, 389 ± 203 for C2, 555 ± 143 for C3 and 583 ±133 for C4). Those values are much higher than mean mixed-layer daytime light intensities, which averaged 151, 170, 140, and 329 µmol photons m^{-2} s^{-1} for C1-C4, respectively. Light intensity and Ek were not correlated. Similarly, no change in the initial slope (α) was observed with changes in mean daytime light intensity. Data on photophysiology will not discussed further, yet we decided to include those data here and in the supplemental material as those datasets can inform the reader on underlying processes of productivity changes and limitations thereof.

4.4. Export Flux

Sediment trap-measured export near the base of the euphotic zone decreased with distance from shore on the P1604 cruise, with values of 20.9, 10.0 and 3.4 mmol C m^{-2} d^{-1} for coastal C4, transition C3, and offshore C2, respectively (Fig. 3). Export efficiency, however, remained relatively constant with distance from shore on this cruise. The *e*-ratio (defined as export/$NPP_{14C,eup}$, where $NPP_{14C,eup}$ is NPP_{14C} integrated to the base of the euphotic zone) was 0.15, 0.14 and 0.15 for C2–C4, respectively. In contrast, export near the base of the euphotic zone showed no clear trend with distance from shore on P1706. Sinking flux was 29.3 mmol C m^{-2} d^{-1} in the coastal C1, 44.5 mmol C m^{-2} d^{-1} in the early filament C2, 35.7 mmol C m^{-2} d^{-1} in the late filament C4, and 46.7 mmol C m^{-2} d^{-1} in transition water C3 (Fig. 4). This led to an inverse relationship between mixed-layer Chl a and the *e*-ratio, with *e*-ratios of 0.05, 0.18, 0.43 and 0.79 for C1–C4, respectively.

4.5. Inter- and Intra-cruise Variability in Production Relationships

Cycle P1604-C2 started in the core of the California Current, and new production was matched by modest NCP values and a diel pattern in the dO_2/Ar measurements (Fig 3 J,L). Overall, P1604-C2 was moderately net autotrophic but, due to the partial depletion of nutrients and change in weather conditions, most production measures showed reduced rates toward the end of the cycle. For P1604-C3, offshore of the coastal boundary in the wind stress curl

upwelling domain, NPP and new production-based estimates increased significantly compared to C2, yet NCP_{prior} was negative at the beginning of the cycle, but became positive around D3. This change in production was correlated with a change in weather as the sea became much calmer and cloud cover was reduced. As expected, productivity was highest in the coastal upwelling region (P1604-C4), where carbon-based production rates tripled. Despite high NO_3^- concentrations, the phytoplankton appeared to utilized NH_4^+ primarily for growth. NCP_{prior} during P1604 indicated that the system was strongly net autotrophic.

Productivity was high where nutrients were plentiful close to shore in the freshly upwelled water of P1706-C1. However, overcast light conditions reduced productivity estimates (except NCP_{prior}) during the early part of this cycle. Comparatively low NP:NPP rate estimates indicate that the phytoplankton community used both ammonia and nitrate as N sources. NCP_{prior} rates averaged 50% of NP, but a distinct diel pattern was observed. P1706-C2 showed reduced production compared to C1, as a result of reduced chlorophyll concentration. Despite lower NPP, NP was higher on day one of C2 compared to C1. NCP analysis indicated that the watermass started to become net heterotrophic at the end of this cycle. P1706-C3 was conducted in a region just outside of the filament where water from the California Current mixed with filament water. P1706-C3 was initially net autotrophic, but production rates were strongly reduced compared to C1 and C2 . The continuous negative trend in NCP was likely driven by horizontal and vertical mixing of different water masses, a deepening of the mixed layer depth over time and the observed decrease of Chl a during this cycle. P1704-C4 was conducted at the location of a drifter that marked the water parcel sampled during C2 and can thus be considered an extension of the previous filament cycle. It was characterized by low chlorophyll despite a nitrate concentration of around 2.9 µM and an ammonium concentration of 1.7 µM. The extremely low NP and the low f-ratio (0.24) also indicate that the phytoplankton community was taking up mostly regenerated N. Further analysis (see discussion below) indicated that cycle 2 was iron limited. NCP rates were found to be near air saturation, indicating that autotrophic and heterotrophic processes were in balance despite the elevated ammonium.

4.5. Production Comparison

The Lagrangian sampling plan and multi-method approach allows us to compare a number of different productivity estimates over a broad range of environmental conditions. We had two

independent estimates of GPP (GPP_{FRRF} and $GPP_{O2/Ar}$), two independent estimates of NPP (NPP_{14C} and $NPP_{G/G}$), and three estimates of NCP or NP (NCP_{prior}, NCP_{RT}, and nitrate uptake), which should be functionally similar to the total exportable carbon produced by the ecosystem. The independent GPP experiments can only be compared for two cycles (P1706-C1 and P1706-C2) because FRRF measurements were not made on the P1604 cruise and because ship movements in and out of the mesoscale filament invalidated $GPP_{O2/Ar}$ assumptions for P1706-C3 and C4. Nonetheless, there is reasonable agreement between the two methods. On P1706-C1, the ratio of GPP_{FRRF}:GPP_{O2Ar} was 0.73, and on P1706-C2 it was 1.32. Agreement was even better for the two NPP measurements, yielding a Pearson's linear correlation of 0.9997 ($p<<10^{-5}$). The mean NPP_{14C} across all paired cycles was 214 mmol C m^{-2} d^{-1}, while the mean $NPP_{G/G}$ was 223 mmol C m^{-2} d^{-1}. Comparing mean NPPs to mean GPPs for P1706-C1 and C2 (941 and 465 mmol C m^{-2} d^{-1} for C1 and C2, respectively), the resulting NPP:GPP ratios are 0.55 and 0.56, respectively, suggesting that 55% of phytoplankton GPP, on average, goes to biomass production. Compared to the agreement between alternate GPP or NPP measurements, the correlation between NCP_{prior} and NCP_{inst} is weak and not statistically significant (Pearson's ρ = 0.60, p = 0.15). This discrepancy was expected, however, as it reflects the different temporal integration scales of NCP_{prior} and NCP_{inst} and the substantial differences in NCP observed in the P1706 filament. There is also substantial discrepancy between NP and the two NCP estimates. The strongest correlation is between NP and NCP_{prior}, though not statistically significant (ρ = 0.52, p = 0.24). NP measurements also substantially exceed those of NCP_{prior} and NCP_{RT}, where mean NCP_{prior} is 8.7 mmol C m^{-2} d^{-1} and mean NP is 73 mmol C m^{-2} d^{-1}.

5. Discussion

The P1604 and P1706 cruises both aimed to measure ecosystem dynamics and biogeochemical rates. P1604 occurred near the end of an anomalously warm period in the northeast Pacific that began with the 2014-2015 North Pacific heat wave and continued with an El Niño in 2015-2016 (Bond et al., 2015; Jacox et al., 2016). At the time of this cruise, much of the region remained above normal temperatures, but upwelling had resumed along the coast, leading to phytoplankton blooms during nearshore experiments P1604-C3 and C4 . P1706 aimed to follow filament transport of freshly upwelled water offshore. Due to this mesoscale focus, P1706 cruise results are substantially influenced by: 1) rapid changes in water column properties

over time; 2) mixing of upwelled and offshore waters during transport; and 3) small-scale spatial gradients in the vicinity of the drift array. In the following discussion, we consider the compatibility and differences among multiple primary production measurements and their applicability in this dynamic region. To compare productivity rate estimates, all data are integrated over the same temporal scale (24 h, cycle duration), analyzed over the mixed layer depth and normalized to carbon units.

5.1. GPP_{FRRF} and $GPP_{O2/Ar}$ Comparisons to NPP

Only recently has it been possible to measure GPP rates with high temporal resolution during research cruises (Hamme et al., 2012; Schuback & Tortell, 2019). Here, we used GPP estimates based on underway FRRF measurements and rates derived from O_2/Ar data. We modified the FRRF method described by Oxborough et al. (2012) to account for potential biases such as noon-time fluorescence quenching and flexible chlorophyll-to-carbon fixation ratios (Schuback et al., 2018). The broader suite of potential corrections as suggested by Boatman et al. (2019) and Schuback et al. (2018) were not available to us during this study. The FRRF data were subsequently compared to the NCP O_2/Ar data from which GPP rates were calculated. As the NCP approach is based on changes of O_2 concentration in the water column, a photosynthetic quotient (PQ; oxygen evolved to carbon fixed) was applied to convert rates into carbon units. Generally, a PQ of 1.4 for NO_3^- supported production and 1.1 for NH_4^+ supported production is used. However, for simplicity and as the PQ can also vary with light induced stress as well as other stress factors, we used a PQ of 1.2 for all samples. Changes in O_2/Ar include all photoautotrophic and heterotrophic activity. Hence, a positive trend during the day indicates that photoautotrophy outweighs all chemoheterotrophy, including phytoplankton respiratory processes. Daytime production includes all respiratory processes and photosynthesis while nighttime data measures only respiratory processes. In order to estimate GPP from diel cycles in O_2/Ar, we assume that the nighttime and daytime respiration rates are equal.

Since no FRRF measurements were conducted during the P1604 cruise, GPP rates were only obtained using the O_2/Ar data. The diurnal rate estimates followed distinct diurnal cycles with a maximum production of around 160 mmol C m^{-2} d^{-1} and a daily average around 40 mmol C m^{-2} d^{-1}. As noted by (Landry et al., 2011a), carbon-based phytoplankton production measured from dilution experiments exceed those from NPP_{14C} because they separately account for

phytoplankton biomass growth and production grazed by microzooplankton over the course of 24-h incubations while NPP_{14C} incorporates respiration losses of grazed ^{14}C-labelled carbon into the measurement. Hence, the difference in portions of GPP recovered by NPP_{14C} and $NPP_{G/G}$ might be interpreted as measure of production losses via food web processes. P1706-C1 and C2 gave high GPP rates for both O_2/Ar and FRRF, with daily mid-day maxima >3000 mmol C m^{-2} d^{-1} for C1 and >1000 mmol C m^{-2} d^{-1} C2. Direct comparison of cycle means indicate that rates were not statistically significantly different between methods ($p \geq 0.4$, t-test, Mann-Whitney Rank Sum test). $GPP_{O2/Ar}$ for P1706-C3 and C4 were compromised by the ship passing through different water masses frequently, which precluded calculating day and night rates for the same water parcel. GPP rates were nonetheless obtained for those cycles from FRRF data. Comparing NPP_{14C} and GPP_{FRRF} estimates for all cycles showed a reasonable % of carbon loss: 36, 51 , 27 and 40 of GPP for P1706-C1-C4, respectively. For the CCE region, ~20% of fixed carbon is released to the DOC pool, with a range between 7 and 44% (Goericke unpublished data; (Stukel et al., 2012)). Respiration alone can also reduce NPP on average by 9 to 22% (López-Sandoval et al., 2014). Higher as well as lower ratios of NPP:GPP have been reported in literature (e.g. Bercel & Kranz, 2019; Kranz et al., 2010). In addition, measured O_2-based GPP estimates that are >200% of simultaneous NPP measurements have been reported in field studies (Hashimoto et al., 2005; Laws et al., 2000). Hence our NPP/GPP ratios fall within expected ranges.

Some uncertainties of the GPP_{FRRF} merit discussion. The GPP_{FRRF} analysis is based on daytime P vs. E curves, but estimates of the photosystem reaction centers (RCII) come from nighttime sampling. Since the number of functional RCII varies throughout the day, over or under estimates of rates may occur. In addition, our calculated GPP rates for the photic zone come solely from phytoplankton sampled at 5-10 m depth. Despite dark or low-light acclimation prior to measurements, the photosystem might not have had time to fully re-oxidized, resulting in underestimates of quantum yield and photochemical production. Moreover, surface communities might express different values in photosynthetic efficiency under low light intensities (α) and maximum photosynthetic rates compared to deep samples. This bias is apparent when analyzing the relatively fast diel changes (Fig. S1), which are likely faster than cell mixing in the water column. Hence, if deeper cells are better adapted to low-light conditions, calculated rates from the mixed layer might be underestimated. Nonetheless, since the MLD was relatively shallow for most cycles, we expect a relatively good estimate. Part of the temporal and spatial mismatch

between GPP_{FRRF} and GPP_{EIMS} might also be explained by likely changes in the electron to C ratios occurring throughout the day which could partially decouple O_2 production from C-fixation. Lastly, due to the lack of pigment data, no spectral correction could be applied to our rate estimates (Schuback et al., 2018). Despite these shortcomings, the good agreement between FRRF and O_2/Ar methods gives us some confidence that both approaches can reliably estimate water-column GPP.

5.2. Net community, New Production and Export Flux

Nitrate consumed by phytoplankton often represents new production in the surface ocean and hence should equate to the amount of organic matter available for export (Eppley & Peterson, 1979), although it may be an overestimate if substantial nitrification occurs within the euphotic zone (Yool et al., 2007). Similarly, NCP represents the balance between organic matter production (photosynthesis) and organic matter consumption (respiration); hence, should also approximate export when the organic pools are at steady-state (Hamme et al., 2012; Li & Cassar, 2017). Crucially, we only expect a quantitative correspondence between NP, NCP and export when integrating over sufficiently long temporal and large spatial scales (Plattner et al., 2005) and including all forms of exported organic matter (Boyd et al., 2019; Ducklow et al., 2001). Comparing these kinds of measurements for short term in-situ or shipboard incubations in spatially heterogeneous regions like the CCE can be challenging to interpret.

Until recently O_2:Ar-based NCP estimates were only used in near-steady-state systems, assuming that timeframes for NCP measurements (weeks to months) need to integrate all past changes in production, grazing and physical disturbances. More recently, Teeter et al. (2018) showed that a strict steady-state assumption for NCP analysis is not required and that reliable rates of NCP can be obtained even if the community varies. This is because the NCP estimate is a weighted analysis of the current oxygen inventory combined with prior gas fluxes for which most weight is placed on the recent past. The weighting reduces historical influence and enhances more recent events. However, the uncertainty of the NCP estimate increases with the physical complexity of a region (Teeter et al., 2018). Due to the complex physical and biochemical nature of the CCE ecosystem, large discrepancies were expected in our method comparison. For example, although upwelling is typically associated with high primary production, the low oxygen content of freshly upwelled waters could be interpreted as negative

NCP. On the other hand, upwelled water with accumulated biomass and high oxygen from the primary production would appear to be strongly net autotrophic, even if NCP had switched to negative. Despite these potential issues, the EIMS method has been usefully applied in other complex coastal environments, such as the Western Antarctic Peninsula (Eveleth et al., 2017; Tortell et al., 2014). Since we applied the EIMS method with a Lagrangian study, we are also able to measure changes in the O_2/Ar ratio with high temporal resolution and resolve some of the uncertainties in measured signal vs. true activity (Teeter et al., 2018; Wang et al., submitted).

Using the calculation of NCP_{inst}, NCP production estimates should match the combined effects of NP and short-term changes in organic matter inventories. Our direct comparison reveals large mismatches, however (Fig 5, Table 1, S4). Four factors play an important role here: 1) NP estimates can never be negative while NCP can be negative, especially in a high-biomass system when grazing exceeds production over the timeframe of measurements; 2) vertical advection or diffusion across isopycnals can introduce low oxygen water into surface layers; 3) NCP rates are influenced by all organisms in the mixed layer, some of which undergo diurnal vertical migration and therefore introduce a vertical transport component to the mass balance; and 4) our Lagrangian approach was partially affected by ship movements during net tows and instrument recovery which introduce a non-lagrangian error into NCP measurements.

As presented in Results, our data show substantial discrepancies between NCP and NP. During P1604-C2 and C4, when regions of high variability were intentionally avoided, there was reasonable agreement, despite statistical differences, between NCP_{RT} and NP measurements (NCP_{inst} = 6.0± 0.1 and NP = 10.6 ± 2.7 mmol C m^{-2} d^{-1} for P1604-C2; NCP_{inst} = 16.4 ± 4.0 and NP = 23.2± 5.9 mmol C m^{-2} d^{-1} for P1604-C4). For P1604-C3, however, NP was relatively high and positive (23.8 ± 8 mmol C m^{-2} d^{-1}) while NCP_{inst} was negative (-0.1 ±1.1 mmol C m^{-2} d^{-1}). On this cycle, surface Chl (1.0 µg L^{-1}), surface NO_3^- (3.8 µmol L^{-1}) and surface POC (7.1 µmol C L^{-1}) were all high, but a dense swarm of doliolids, with high grazing and presumably high respiration, dominated the zooplankton (Morrow et al., 2018). It is thus likely that the discrepancy in P1604-C3 measurements was due to a system in which NCP and NP were temporarily decoupled, with nitrate fueling substantial NP even as high mesozooplankton grazing and respiration drove NCP towards net heterotrophy.

For P1706, the differences between NCP and NP were more pronounced. NP was reasonably high on all cycles, with mean *f*-ratios varying from 0.27 to 0.49. NCP_{inst} was high on P1706-C1 (although still only 49% of NP), but negative or near zero on all other cycles. These results might be explained by the unusual physical and biological dynamics of the mesoscale filament that was studied on this cruise. Specifically, the cruise targeted non-steady-state water parcels ranging from coastal upwelling on C1 to aged filament water mixed with offshore California Current water on C3, as well as water parcels during early and late stages of a filament evolution (P1706-C2 and C4). Along this continuum from upwelling to offshore mixing, surface POC declined substantially from 38.5 to 5.7 µmol C L^{-1} for P1706-C1 to C4. This biomass decline (during offshore transit over 2-3 weeks) would have to be matched by a combination of export and/or negative NCP along the transect. However, NP cannot be negative, and although NO_3^- decreased from inshore to offshore, surface nitrate remained relatively high (2.9 µmol C L^{-1}) allowing continued new production. Ammonium also accumulated between P1706-C1 and P1706-C4 (from 0.4 to 1.8 µmol L^{-1}), as would be expected if remineralization exceeded phytoplankton production**.** Our results are thus consistent with a system in which NCP peaked early in the bloom and switched to negative as the bloom declined. A similar NP and NCP pattern was observed following a coastal Antarctic bloom (Stukel et al., 2015b; Tortell et al., 2014). The NCP estimates could also have been affected by upwelling and/or vertical diffusion in this energetic mesoscale environment, which would underestimate NCP if low O_2 water was introduced from below the mixed layer (see Wang et al. (submitted) for potential impact on NCP). In addition, nitrate uptake could overestimate NP if substantial nitrification occurs in the euphotic zone. This would seem an unlikely scenario, given estimates of mixed-layer nitrification in the CCE (4.6 nmol L^{-1} d^{-1}; (Santoro et al., 2013) that are relatively low compared to nitrate uptake rates. However, nitrification might be more active in filaments.

Ultimately, NP and NCP should be balanced by export production. Our results show, however, that export flux was substantially lower than NP across the region (Fig. 5). When integrated to the base of the euphotic zone (data not shown) to match sediment trap data, NP exceeded export for all three cycles of P1604 and for all cycles of P1706 except C4 (at the end of the filament). For all the cycles of P1706, NP averaged 2.7 times higher than sinking flux. The same pattern did not hold for NCP in P1706 because of multiple cycles with negative NCP. In a non-steady state system, however, export should be balanced not by NCP alone, but by the sum of NCP and

POC decline, unless large parts of NCP are also going into DOC buildup. Because P1706-C4 was a transport extension of C2, we can test this balance over the 12 days that separate the beginning and end of those cycles. Over this period, POC declined from 1078 to 510 mmol C m^{-2}, equating to a decline of 43.6 mmol C m^{-2} d^{-1}. This is remarkably similar to the mean export during these two cycles (40.1 mmol C m^{-2} d^{-1}), suggesting that the declining biomass would have been sufficient to support all the measured export flux even if no additional biomass was produced.

The measurement of new production in excess of sinking flux is not a novel result. Nitrate uptake has also been reported to exceed the sinking particle export in the Western Antarctic Peninsula (Ducklow et al., 2018; Stukel et al., 2015a), the Bermuda Atlantic Time-Series site (Lipschultz, 2001; Lomas et al., 2013), the Arabian Sea (Buesseler et al., 1998; Sambrotto, 2001), and the Costa Rica Dome (Stukel et al., 2016). In addition, NCP has been found to exceed sinking flux in the Sargasso Sea (Estapa et al., 2015) and the Western Antarctic Peninsula (Stukel et al., 2015a). Within the CCE, prior studies have determined e-ratios of ~0.2 (Kelly et al., 2018), compared to *f*-ratios frequently >0.5 (Harrison et al., 1987) and a region-wide NCP/NPP ratio of 0.4 (Munro et al., 2013). This deficiency of sinking export relative to NP and NCP likely reflects the importance of non-sinking forms of export including active transport of carbon by diel vertical migrants (Bianchi et al., 2013; Steinberg et al., 2000) and subduction of particulate and dissolved organic matter (Carlson et al., 1994; Omand et al., 2015). Within the CCE, subduction of particles has been shown to be a substantial flux of organic matter out of the euphotic zone, although subducted particles did not penetrate deep into the ocean interior (Stukel et al., 2018). Active transport has also been shown to be substantial, and even to rival sinking flux, in high biomass regions of the CCE (Kelly et al., 2019). Together, these other processes likely explain our measurement discrepancies between NP and export.

6. Conclusions

Our study presents a well-constrained characterization of gross primary production, net primary production, net community production, new production, and export production in a complex and heterogeneous physical environment. The results show how a multi-method approach can clarify some of the variabilities and inconsistencies observed using different methods. We found strong spatial gradients in productivity rates from coastal to offshore regions

that were primarily driven by decreasing biomass and nutrient availability with distance from shore and we showed that the high-resolution measurements applied here resolved diel patterns in GPP and NCP. Overall, all our data from temporally resolved production estimates are surprisingly consistent, within the errors of the estimates, with data from traditional 24-h production measurements. The GPP:NPP ratio was approximately 2 over the study region, with no distinct spatial pattern. The *f*-ratios (NP:NPP) varied from 0.16 to 0.55, suggesting that recycled NH_4^+ was typically the most important nutrient supporting production, even though nitrate was still a major source of N. New production typically exceeded carbon export of sinking particles by a large margin, suggesting that temporally and spatially decoupled export (vertical migration of grazers, water mass subduction) must be quantitatively important for resolving the region's carbon budget. Since underway high temporal resolution analyses of productivity using FRRF and EIMS match general ecosystem expectations, we suggest that temporally resolved production methods should be employed regularly to enhance understanding of physically complex and economically important ecosystems.

7. Acknowledgements, Samples and Data:

The authors declare no conflict of interest. Data reported and presented in this study can be accessed at the CCE-LTER Datazoo online database (archiving is underway during the manuscript review process).

This study was funded by US National Science Foundation grants OCE-1637632 (CCE-LTER) and -1614359 (RAPID). We appreciate the contributions to shipboard sampling and analyses by Ali Freibott, Belli Valencia, Shonna Dovel and Megan Roadman and Cameron Quackenbush. We also want to thank the captains and the crews of the *R/V Sikuliaq* and *R/V Roger Revelle* for their support. We appreciated the help during both cruises by Chief scientist Mark Ohman. We also want to thank Kathy Barbeau and Kiefer Forsch for their discussion of their preliminary data on iron limitation during these cruises.

References

Barron, R. K., Siegel, D. A., & Guillocheau, N. (2014). Evaluating the importance of phytoplankton community structure to the optical properties of the Santa Barbara Channel, California. *Limnology and Oceanography, 59*(3), 927-946.

Behrenfeld, M. J., & Falkowski, P. G. (1997). Photosynthetic rates derived from satellite-based chlorophyll concentration. *Limnology and Oceanography, 42*(1), 1-20.

Bercel, T. L., & Kranz, S. A. (2019). Insights into carbon acquisition and photosynthesis in Karenia brevis under a range of CO2 concentrations. *Progress in Oceanography, 172*, 65-76.

Bianchi, D., Stock, C., Galbraith, E. D., & Sarmiento, J. L. (2013). Diel vertical migration: Ecological controls and impacts on the biological pump in a one-dimensional ocean model. *Global Biogeochemical Cycles, 27*(2), 478-491.

Boatman, T. G., Geider, R. J., & Oxborough, K. (2019). Improving the accuracy of single turnover active fluorometry (STAF) for the estimation of phytoplankton primary productivity (PhytoPP). *bioRxiv*, 583591.

Bond, N. A., Cronin, M. F., Freeland, H., & Mantua, N. (2015). Causes and impacts of the 2014 warm anomaly in the NE Pacific. *Geophysical Research Letters, 42*(9), 3414-3420.

Boyd, P. W., Claustre, H., Levy, M., Siegel, D. A., & Weber, T. (2019). Multi-faceted particle pumps drive carbon sequestration in the ocean. *Nature, 568*(7752), 327-335.

Bronk, D. A., Glibert, P. M., & Ward, B. B. (1994). Nitrogen uptake, dissolved organic nitrogen release, and new production. *Science, 265*(5180), 1843-1846.

Buesseler, K., Ball, L., Andrews, J., Benitez-Nelson, C., Belastock, R., Chai, F., & Chao, Y. (1998). Upper ocean export of particulate organic carbon in the Arabian Sea derived from thorium-234. *Deep-Sea Research II, 45*(10-11), 2461-2487.

Carlson, C. A., Ducklow, H. W., & Michaels, A. F. (1994). Annual Flux of Dissolved Organic-Carbon from the Euphotic Zone in the Northwestern Sargasso Sea. *Nature, 371*(6496), 405-408.

Cassar, N., Barnett, B. A., Bender, M. L., Kaiser, J., Hamme, R. C., & Tilbrook, B. (2009). Continuous high-frequency dissolved O2/Ar measurements by equilibrator inlet mass spectrometry. *Analytical Chemistry, 81*(5), 1855-1864.

Chavez, F. P., & Messie, M. (2009). A comparison of Eastern Boundary Upwelling Ecosystems. *Progress in Oceanography, 83*(1-4), 80-96.

Collos, Y. (1998). Nitrate uptake, nitrite release and uptake, and new production estimates. *Marine Ecology Progress Series, 171*, 293-301.

Ducklow, H. W., Steinberg, D. K., & Buesseler, K. O. (2001). Upper ocean carbon export and the biological pump. . *Oceanography 14*(4), 0–58.

Ducklow, H. W., Stukel, M. R., Eveleth, R., Doney, S. C., Jickells, T., Schofield, O., et al. (2018). Spring-summer net community production, new production, particle export and related water column biogeochemical processes in the marginal sea ice zone of the Western Antarctic Peninsula 2012-2014. *Philosophical Transactions of the Royal Society a-Mathematical Physical and Engineering Sciences, 376*(2122).

Dugdale, R. C. (1972). Chemical oceanography and primary productivity in upwelling regions. *Geoforum, 3*(3), 47-61.

Dugdale, R. C., & Goering, J. J. (1967). Uptake of New and Regenerated Forms of Nitrogen in Primary Productivity. *Limnology and Oceanography, 12*(2), 196-206.

Dugdale, R. C., & Wilkerson, F. P. (1986). The Use of ^{15}N to Measure Nitrogen Uptake in Eutrophic Oceans - Experimental Considerations. *Limnology and Oceanography, 31*(4), 673-689.

Dunne, J. P., Sarmiento, J. L., & Gnanadesikan, A. (2007). A synthesis of global particle export from the surface ocean and cycling through the ocean interior and on the seafloor. *Global Biogeochemical Cycles, 21*(4).

Eppley, R. W., & Peterson, B. J. (1979). Particulate Organic-Matter Flux and Planktonic New Production in the Deep Ocean. *Nature, 282*(5740), 677-680.

Estapa, M. L., Siegel, D. A., Buesseler, K. O., Stanley, R. H. R., Lomas, M. W., & Nelson, N. B. (2015). Decoupling of net community and export production on submesoscales. *Global Biogeochemical Cycles, 29*(8), 1266-1282.

Eveleth, R., Cassar, N., Doney, S. C., Munro, D. R., & Sweeney, C. (2017). Biological and physical controls on O_2/Ar, Ar and pCO_2 variability at the Western Antarctic Peninsula and in the Drake Passage. *Deep Sea Research II, 139*, 77-88.

Falkowski, P. G., & Kolber, Z. (1993). *Estimation of Phytoplankton Photosynthesis by Active Fluorescence.* Paper presented at the Measurement of Primary Production from the Molecular to the Global Scale.

Goldman, J. A. L., Kranz, S. A., Young, J. N., Tortell, P. D., Stanley, R. H. R., Bender, M. L., & Morel, F. M. M. (2015). Gross and net production during the spring bloom along the Western Antarctic Peninsula. *New Phytologist, 205*(1), 182-191.

Gordon, L. I., Jennings, J. C., Ross, A. A., & Krest, J. M. (1992). A suggested Protocol for Continuous Flow Automated Analysis of Seawater Nutrients in the WOCE Hydrographic Program and the Joint Global Ocean Fluxes Study *Grp. Tech Rpt OSU College of Oceanography Descr. Chem Oc., 92*(1).

Hamme, R. C., Cassar, N., Lance, V. P., Vaillancourt, R. D., Bender, M. L., Strutton, P. G., et al. (2012). Dissolved O_2/Ar and other methods reveal rapid changes in productivity during a Lagrangian experiment in the Southern Ocean. *Journal of Geophysical Research-Oceans, 117*(C4).

Harrison, W. G., Platt, T., & Lewis, M. R. (1987). F-Ratio and Its Relationship to Ambient Nitrate Concentration in Coastal Waters. *Journal of Plankton Research, 9*(1), 235-248.

Hashimoto, S., Horimoto, N., Yamaguchi, Y., Ishimaru, T., & Saino, T. (2005). Relationship between net and gross primary production in the Sagami Bay, Japan. *Limnology and Oceanography, 50*(6), 1830-1835.

Jacox, M. G., Hazen, E. L., Zaba, K. D., Rudnick, D. L., Edwards, C. A., Moore, A. M., & Bograd, S. J. (2016). Impacts of the 2015-2016 El Nino on the California Current System: Early assessment and comparison to past events. *Geophysical Research Letters, 43*(13), 7072-7080.

Kahru, M., Jacox, M. G., Lee, Z., Kudela, R. M., Manzano-Sarabia, M., & Mitchell, B. G. (2015). Optimized multi-satellite merger of primary production estimates in the California Current using inherent optical properties. *Journal of Marine Systems, 147*, 94-102.

Kanda, J., Itoh, T., Ishikawa, D., & Watanabe, Y. (2003). Environmental control of nitrate uptake in the East China Sea. *Deep-Sea Research II, 50*(2), 403-422.

Kelly, T. B., Davison, P. C., Goericke, R., Landry, M. R., Ohman, M. D., & Stukel, M. R. (2019). The Importance of Mesozooplankton Diel Vertical Migration for Sustaining a Mesopelagic Food Web. *bioRxiv*, 642975.

Kelly, T. B., Goericke, R., Kahru, M., Song, H., & Stukel, M. R. (2018). CCE II: Spatial and interannual variability in export efficiency and the biological pump in an eastern boundary current upwelling system with substantial lateral advection. *Deep-Sea Research I 140*, 14-25.

Knauer, G. A., Martin, J. H., & Bruland, K. W. (1979). Fluxes of Particulate Carbon, Nitrogen, and Phosphorus in the Upper Water Column of the Northeast Pacific. *Deep-Sea Research I 26*(1), 97-108.

Kolber, Z., & Falkowski, P. G. (1993). Use of Active Fluorescence to Estimate Phytoplankton Photosynthesis in-Situ. *Limnology and Oceanography, 38*(8), 1646-1665.

Kolber, Z. S., Barber, R. T., Coale, K. H., Fitzwater, S. E., Greene, R. M., Johnson, K. S., et al. (1994). Iron Limitation of Phytoplankton Photosynthesis in the Equatorial Pacific-Ocean. *Nature, 371*(6493), 145-149.

Kranz, S. A., Levitan, O., Richter, K.-U., Prasil, O., Berman-Frank, I., & Rost, B. (2010). Combined effects of CO_2 and light on the N_2-fixing cyanobacterium *Trichodesmium* IMS101: Physiological responses. *Plant Physiology 154*(1), 334-345.

Kudela, R. M., Banas, N. S., Barth, J. A., Frame, E. R., Jay, D. A., Largier, J. L., et al. (2008). New Insights into the Controls and Mechanisms of Plankton Productivity in Coastal Upwelling Waters of the Northern California Current System. *Oceanography, 21*(4), 46-59.

Kumar, N., Anderson, R. F., Mortlock, R. A., Froelich, P. N., Kubik, P., Dittrichhannen, B., & Suter, M. (1995). Increased Biological Productivity and Export Production in the Glacial Southern-Ocean. *Nature, 378*(6558), 675-680.

Landry, M. R., Brown, S. L., Rii, Y. M., Selph, K. E., Bidigare, R. R., Yang, E. J., & Simmons, M. P. (2008). Depth-stratified phytoplankton dynamics in Cyclone Opal, a subtropical mesoscale eddy. *Deep-Sea Research II, 55*(10-13), 1348-1359.

Landry, M. R., Constantinou, J., Latasa, M., Brown, S. L., Bidigare, R. R., & Ondrusek, M. E. (2000). Biological response to iron fertilization in the eastern equatorial Pacific (IronEx II). III. Dynamics of phytoplankton growth and microzooplankton grazing. *Marine Ecology Progress Series, 201*, 57-72.

Landry, M. R., & Hassett, R. P. (1982). Estimating the Grazing Impact of Marine Micro-Zooplankton. *Marine Biology, 67*(3), 283-288.

Landry, M. R., Ohman, M. D., Goericke, R., Stukel, M. R., Barbeau, K. A., Bundy, R., & Kahru, M. (2012). Pelagic community responses to a deep-water front in the California

Current Ecosystem: overview of the A-Front Study. *Journal of Plankton Research, 34*(9), 739-748.

Landry, M. R., Selph, K. E., Decima, M., Gutierrez-Rodriguez, A., Stukel, M. R., Taylor, A. G., & Pasulka, A. L. (2016). Phytoplankton production and grazing balances in the Costa Rica Dome. *Journal of Plankton Research, 38*(2), 366-379.

Landry, M. R., Selph, K. E., Taylor, A. G., Decima, M., Balch, W. M., & Bidigare, R. R. (2011a). Phytoplankton growth, grazing and production balances in the HNLC equatorial Pacific. *Deep-Sea Research II, 58*(3-4), 524-535.

Landry, M. R., Selph, K. E., & Yang, E. J. (2011b). Decoupled phytoplankton growth and microzooplankton grazing in the deep euphotic zone of the eastern equatorial Pacific. *Marine Ecology Progress Series, 421*, 13-24.

Lawrenz, E., Silsbe, G., Capuzzo, E., Ylostalo, P., Forster, R. M., Simis, S. G. H., et al. (2013). Predicting the Electron Requirement for Carbon Fixation in Seas and Oceans. *PLoS ONE, 8*(3).

Laws, E. A., Landry, M. R., Barber, R. T., Campbell, L., Dickson, M. L., & Marra, J. (2000). Carbon cycling in primary production bottle incubations: inferences from grazing experiments and photosynthetic studies using (14)C and (18)O in the Arabian Sea. *Deep-Sea Research II, 47*(7-8), 1339-1352.

Li, Q. P., Franks, P. J. S., Landry, M. R., Goericke, R., & Taylor, A. G. (2010). Modeling phytoplankton growth rates and chlorophyll to carbon ratios in California coastal and pelagic ecosystems. *Journal of Geophysical Research-Biogeosciences, 115*.

Li, Z. C., & Cassar, N. (2017). A mechanistic model of an upper bound on oceanic carbon export as a function of mixed layer depth and temperature. *Biogeosciences, 14*(22), 5015-5027.

Lipschultz, F. (2001). A time-series assessment of the nitrogen cycle at BATS. *Deep-Sea Research II, 48*(8-9), 1897-1924.

Lomas, M. W., Bates, N. R., Johnson, R. J., Knap, A. H., Steinberg, D. K., & Carlson, C. A. (2013). Two decades and counting: 24-years of sustained open ocean biogeochemical measurements in the Sargasso Sea. *Deep-Sea Research II, 93*, 16-32.

Longhurst, A., Sathyendranath, S., Platt, T., & Caverhill, C. (1995). An Estimate of Global Primary Production in the Ocean from Satellite Radiometer Data. *Journal of Plankton Research, 17*(6), 1245-1271.

López-Sandoval, D. C., Rodríguez-Ramos, T., Cermeño, P., Sobrino, C., & Marañón, E. (2014). Photosynthesis and respiration in marine phytoplankton: Relationship with cell size, taxonomic affiliation, and growth phase. *Journal of Experimental Marine Biology and Ecology, 457*, 151-159.

Luz, B., & Barkan, E. (2005). The isotopic ratios $^{17}O/^{16}O$ and $^{18}O/^{16}O$ in molecular oxygen and their significance in biogeochemistry. *Geochimica et Cosmochimica Acta, 69*(5), 1099-1110.

Marra, J. (2009). Net and gross productivity: Weighing in with 14C. *Aquatic Microbial Ecology 56*(2), 123-131
.

Michaels, A. F., & Silver, M. W. (1988). Primary Production, Sinking Fluxes and the Microbial Food Web. *Deep-Sea Research I 35*(4), 473-490.

Moore, C. M., Suggett, D. J., Hickman, A. E., Kim, Y. N., Tweddle, J. F., Sharples, J., et al. (2006). Phytoplankton photoacclimation and photoadaptation in response to environmental gradients in a shelf sea. *Limnology and Oceanography, 51*(2), 936-949.

Morrow, R. M., Ohman, M. D., Goericke, R., Kelly, T. B., Stephens, B. M., & Stukel, M. R. (2018). CCE V: Primary production, mesozooplankton grazing, and the biological pump in the California Current Ecosystem: Variability and response to El Nino. *Deep-Sea Research I 140*, 52-62.

Muller-Karger, F. E., Varela, R., Thunell, R., Luerssen, R., Hu, C. M., & Walsh, J. J. (2005). The importance of continental margins in the global carbon cycle. *Geophysical Research Letters, 32*(1).

Munro, D. R., Quay, P. D., Juranek, L. W., & Goericke, R. (2013). Biological production rates off the Southern California coast estimated from triple O_2 isotopes and O_2 : Ar gas ratios. *Limnology and Oceanography, 58*(4), 1312-1328.

Myklestad, S. M. (2000). *The Handbook of Environmental Chemistry* (Vol. Vol. 5D): Springer.

Nagai, T., Gruber, N., Frenzel, H., Lachkar, Z., McWilliams, J. C., & Plattner, G. K. (2015). Dominant role of eddies and filaments in the offshore transport of carbon and nutrients in the California Current System. *Journal of Geophysical Research-Oceans, 120*(8), 5318-5341.

Nickels, C. F., & Ohman, M. D. (2018). CCEIII: Persistent functional relationships between copepod egg production rates and food concentration through anomalously warm conditions in the California Current Ecosystem. *Deep-Sea Research I 140*, 26-35.

O'Reilly, J. E., Maritorena, S., Mitchell, B. G., Siegel, D. A., Carder, K. L., Garver, S. A., et al. (1998). Ocean color chlorophyll algorithms for SeaWiFS. *Journal of Geophysical Research-Oceans, 103*(C11), 24937-24953.

Ohman, M. D., Powell, J. R., Picheral, M., & Jensen, D. W. (2012). Mesozooplankton and particulate matter responses to a deep-water frontal system in the southern California Current System. *Journal of Plankton Research, 34*(9), 815-827.

Omand, M. M., D'Asaro, E. A., Lee, C. M., Perry, M. J., Briggs, N., Cetinic, I., & Mahadevan, A. (2015). Eddy-driven subduction exports particulate organic carbon from the spring bloom. *Science, 348*(6231), 222-225.

Oxborough, K., Moore, C. M., Suggett, D. J., Lawson, T., Chan, H. G., & Geider, R. J. (2012). Direct estimation of functional PSII reaction center concentration and PSII electron flux on a volume basis: a new approach to the analysis of Fast Repetition

Rate fluorometry (FRRf) data. *Limnology and Oceanography-Methods, 10*, 142-154.

Painter, S. C., Sanders, R., Poulton, A. J., Woodward, E. M. S., Lucas, M., & Chamberlain, K. (2007). Nitrate uptake at photic zone depths is not important for export in the subtropical ocean. *Global Biogeochemical Cycles, 21*(4).

Pan, X. J., Mannino, A., Marshall, H. G., Filippino, K. C., & Mulholland, M. R. (2011). Remote sensing of phytoplankton community composition along the northeast coast of the United States. *Remote Sensing of Environment, 115*(12), 3731-3747.

Peterson, B. J. (1980). Aquatic Primary Productivity and the C_{14}-CO_2 Method - a History of the Productivity Problem. *Annual Review of Ecology and Systematics, 11*, 359-385.

Platt, T., Gallegos, C. L., & Harrison, W. G. (1980). Photoinhibition of Photosynthesis in Natural Assemblages of Marine-Phytoplankton. *Journal of Marine Research, 38*(4), 687-701.

Plattner, G. K., Gruber, N., Frenzel, H., & McWilliams, J. C. (2005). Decoupling marine export production from new production. *Geophysical Research Letters, 32*(11).

Quay, P. D., Peacock, C., Bjorkman, K., & Karl, D. M. (2010). Measuring primary production rates in the ocean: Enigmatic results between incubation and non-incubation methods at Station ALOHA. *Global Biogeochemical Cycles, 24*.

Reuer, M. K., Barnett, B. A., Bender, M. L., Falkowski, P. G., & Hendricks, M. B. (2007). New estimates of Southern Ocean biological production rates from O-2/Ar ratios and the triple isotope composition of O-2. *Deep-Sea Research I 54*(6), 951-974.

Robinson, C., Tilstone, G. H., Rees, A. P., Smyth, T. J., Fishwick, J. R., Tarran, G. A., et al. (2009). Comparison of in vitro and in situ plankton production determinations. *Aquatic Microbial Ecology, 54*(1), 13-34.

Saba, V. S., Friedrichs, M. A. M., Antoine, D., Armstrong, R. A., Asanuma, I., Behrenfeld, M. J., et al. (2011). An evaluation of ocean color model estimates of marine primary

productivity in coastal and pelagic regions across the globe. *Biogeosciences, 8*(2), 489-503.

Sambrotto, R. N. (2001). Nitrogen production in the northern Arabian Sea during the Spring Intermonsoon and Southwest Monsoon seasons. *Deep-Sea Research II, 48*(6-7), 1173-1198.

Santoro, A. E., Sakamoto, C. M., Smith, J. M., Plant, J. N., Gehman, A. L., Worden, A. Z., et al. (2013). Measurements of nitrite production in and around the primary nitrite maximum in the central California Current. *Biogeosciences, 10*(11), 7395-7410.

Schuback, N., Hoppe, C. J. M., Tremblay, J. E., Maldonado, M. T., & Tortell, P. D. (2018). Primary productivity and the coupling of photosynthetic electron transport and carbon fixation in the Arctic Ocean (vol 62, pg 898, 2017). *Limnology and Oceanography, 63*(3), 1444-1444.

Schuback, N., & Tortell, P. D. (2019). Diurnal regulation of photosynthetic light absorption, electron transport and carbon fixation in two contrasting oceanic environments. *Biogeosciences, 16*(7), 1381-1399.

Steemann Nielsen, E. (1952). he Use of Radio-active Carbon (C14) for Measuring Organic Production in the Sea. *ICES Journal of Marine Science, 18*(2), 117-140.

Steinberg, D. K., Carlson, C. A., Bates, N. R., Goldthwait, S. A., Madin, L. P., & Michaels, A. F. (2000). Zooplankton vertical migration and the active transport of dissolved organic and inorganic carbon in the Sargasso Sea. *Deep-Sea Research I 47*(1), 137-158.

Stock, C., & Dunne, J. (2010). Controls on the ratio of mesozooplankton production to primary production in marine ecosystems. *Deep-Sea Research I, 57*(1), 95-112.

Strickland, J. D., & Parsons, T. R. (1972). A practical handbook of seawater analysis, second ed. *Bulletin of the Fisheries Research Board of Canada, 167*.

Stukel, M. R., Asher, E., Couto, N., Schofield, O., Strebel, S., Tortell, P., & Ducklow, H. W. (2015a). The imbalance of new and export production in the western Antarctic Peninsula, a potentially "leaky" ecosystem. *Global Biogeochemical Cycles, 29*(9), 1400-1420.

Stukel, M. R., Benitez-Nelson, C. R., Decima, M., Taylor, A. G., Buchwald, C., & Landry, M. R. (2016). The biological pump in the Costa Rica Dome: an open-ocean upwelling system with high new production and low export. *Journal of Plankton Research, 38*(2), 348-365.

Stukel, M. R., Goericke, R., & Landry, M. R. (2019a). Predicting primary production in the southern California Current Ecosystem from chlorophyll, nutrient concentrations, and irradiance. *bioRxiv*, 590240.

Stukel, M. R., Kahru, M., Benitez-Nelson, C. R., Decima, M., Goericke, R., Landry, M. R., & Ohman, M. D. (2015b). Using Lagrangian-based process studies to test satellite algorithms of vertical carbon flux in the eastern North Pacific Ocean. *Journal of Geophysical Research-Oceans, 120*(11), 7208-7222.

Stukel, M. R., Kelly, T. B., Aluwihare, L. I., Barbeau, K. A., Goericke, R., Krause, J. W., et al. (2019b). The Carbon:(234)Thorium ratios of sinking particles in the California current ecosystem 1: relationships with plankton ecosystem dynamics. *Marine chemistry, 212*, 1-15.

Stukel, M. R., Landry, M. R., Ohman, M. D., Goericke, R., Samo, T., & Benitez-Nelson, C. R. (2012). Do inverse ecosystem models accurately reconstruct plankton trophic flows? Comparing two solution methods using field data from the California Current. *Journal of Marine Systems, 91*(1), 20-33.

Stukel, M. R., Ohman, M. D., Benitez-Nelson, C. R., & Landry, M. R. (2013). Contributions of mesozooplankton to vertical carbon export in a coastal upwelling system. *Marine Ecology Progress Series, 491*, 47-+.

Stukel, M. R., Song, H., Goericke, R., & Miller, A. J. (2018). The role of subduction and gravitational sinking in particle export, carbon sequestration, and the remineralization length scale in the California Current Ecosystem. *Limnology and Oceanography*, *63*(1), 363-383.

Suggett, D., Kraay, G., Holligan, P., Davey, M., Aiken, J., & Geider, R. (2001). Assessment of photosynthesis in a spring cyanobacterial bloom by use of a fast repetition rate fluorometer. *Limnology and Oceanography*, *46*(4), 802-810.

Teeter, L., Hamme, R. C., Ianson, D., & Bianucci, L. (2018). Accurate Estimation of Net Community Production From O-2/Ar Measurements. *Global Biogeochemical Cycles*, *32*(8), 1163-1181.

Teira, E., José Pazó, M., Serret, P., & Fernández, E. (2001). Dissolved organic carbon production by microbial populations in the Atlantic Ocean. *Limnology and Oceanography*, *46*(6), 1370-1377.

Thunell, R., Benitez-Nelson, C., Varela, R., Astor, Y., & Muller-Karger, F. (2007). Particulate organic carbon fluxes along upwelling-dominated continental margins: Rates and mechanisms. *Global Biogeochemical Cycles*, *21*(1).

Tortell, P. D., Asher, E. C., Ducklow, H. W., Goldman, J. A. L., Dacey, J. W. H., Grzymski, J. J., et al. (2014). Metabolic balance of coastal Antarctic waters revealed by autonomous pCO_2 and Delta O_2/Ar measurements. *Geophysical Research Letters*, *41*(19), 6803-6810.

Uitz, J., Stramski, D., Reynolds, R. A., & Dubranna, J. (2015). Assessing phytoplankton community composition from hyperspectral measurements of phytoplankton absorption coefficient and remote-sensing reflectance in open-ocean environments. *Remote Sensing of Environment*, *171*, 58-74.

Wang, S., Kranz, S. A., Kelly, T. B., Song, H., R., S. M., & N., C. (submitted). Lagrangian studies of net community production: The effect of diel and multi-day non-steady

state factors and vertical fluxes on O2/Ar in a dynamic upwelling region. *JGR-Oceans*.

Yool, A., Martin, A. P., Fernandez, C., & Clark, D. R. (2007). The significance of nitrification for oceanic new production. *Nature*, *447*(7147), 999-1002.

Table 1: Production metrics for CCL-LTER Process cruises P1604 and P1706. Values represent average rates in mmol C m^{-2} d^{-1} integrated over the mixed layer depth. Errors are standard errors of the mean (SOM). ND indicates that no measurements were made. X indicates that data were not reliable as indicated in the text.

	NCP Prior	NCP inst	NPP_{14C}	$NPP_{G/G}$	NP	Export flux	f-ratio	GPP (FRRF)	GPP-EIMS	Respiration (EIMS)
P1604										
Cycle 2	5.51 ± 0.25	6.02 ± -0.13	17.7 ± 4.5	35.0 ± 5.8	10.6 ± 2.7	3.4	0.55 ± 0.06	ND	42.25 ± 9.3	57.25 ± 3
Cycle_3	-0.59 ± 5.61	-0.13 ± 1.18	48.4 ± 8.4	61.9 ± 7.8	23.9±8.0	10.0	0.44 ± 0.07	ND	124± X	131 ± X
Cycle_4	39.47 ± 3.99	16.37 ± 4.04	126.4± 23.4	ND	22.9 ± 5.9	20.9	0.16 ± 0.01	ND	348± 158	418.35 ± 190.16
P1706										
Cycle 1	58.89 ± 1.24	77.84 ± 0.5	511.5± 150.1	524.1 ± 142.1	156.8 ± 19.2	29.3	0.34 ± 0.09	799.34 ± 158	1082 ±134	1278.67 ± 76.93
Cycle_2	-12.23 ± 8.57	-14.26 ± 11.32	256.3 ± 27.9	269.2 ± 44.1	101.6 ± 44.0	44.5	0.40 ± 0.14	529.50 ± 97	401.1 ±52.3	554.25± 101.32
Cycle 3	-11.8 ± 33.05	-10.47 ± 4.29	70.4± 21.9	76.7 ± 39.1	29.3± 18.5	46.7	0.49 ± 0.26	96.13 ± 20	X	X
Cycle_4	-0.19 ± 1.16	-0.07 ± 0.28	18.5±X	22.00 ± 6.4	5.4± 0.1	35.7	0.27 ± X	30.64 ± 1	X	X

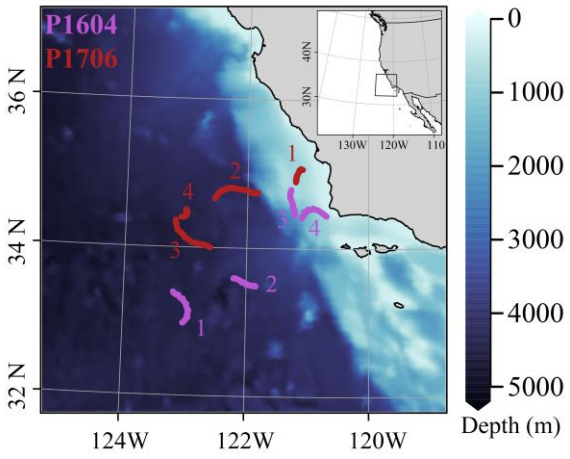

Figure 1. Map of Lagrangian study sites for cruises P1604 (purple) and P1706 (red). P1604 started in the west offshore and continues inshore, P1706 started in the east and continues further offshore. Colors indicate bathymetry.

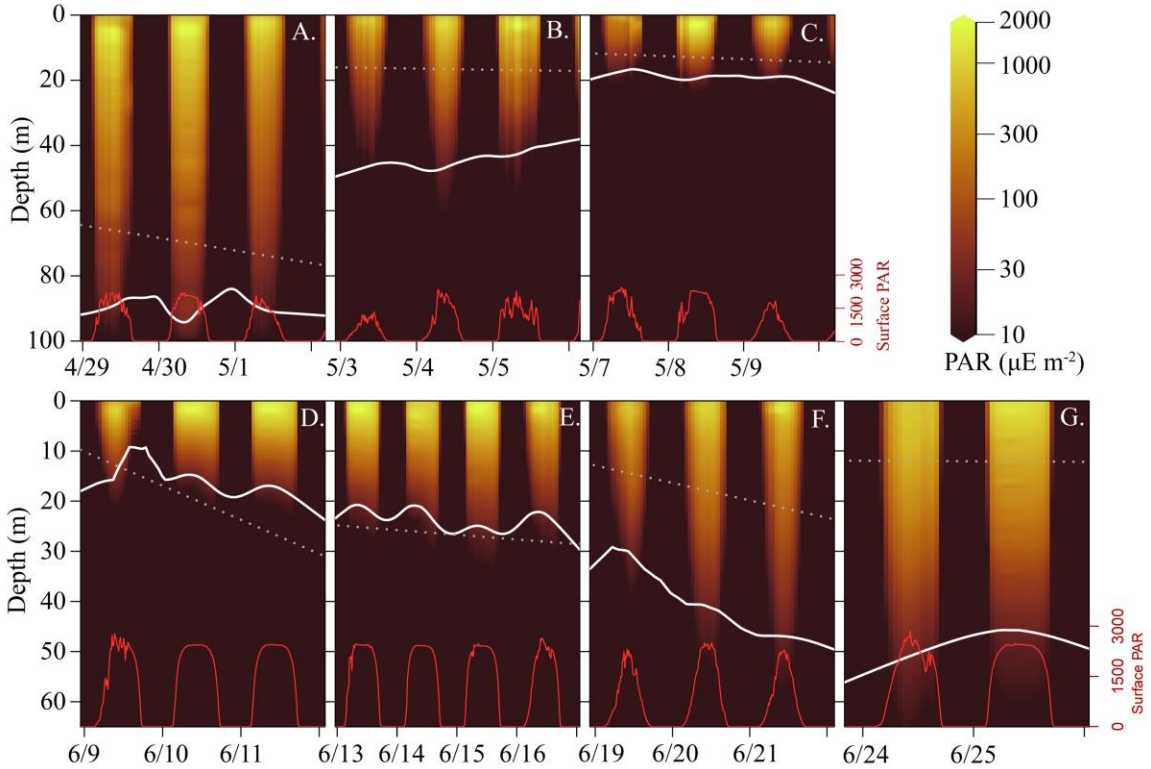

Figure 2. Mixed layer depth and light levels for all experimental cycles (A. P1604-C2, B. P1604-C3, C. P1604-C4, D. P1706-C1, E. P1706-C2, F. P1706-C3, G. P1706-C4). Red lines indicate surface PAR intensity, colored shading indicate water-column light intensity (µmol photons $m^{-2}s^{-1}$), white solid line indicates depth of the 1% light level, and dotted line indicates the mixed layer depth.

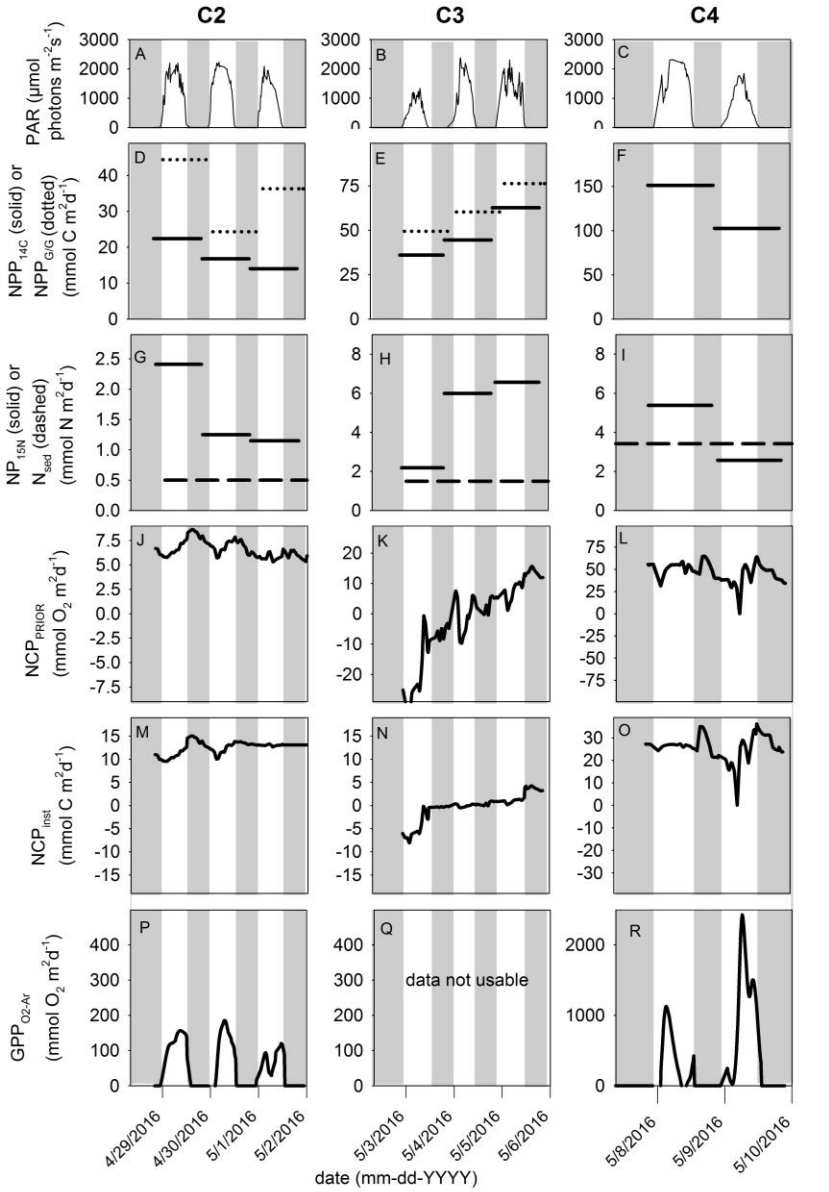

Figure 3. Chronology of primary production estimates during P1604. Panels [A-C] depict light intensity during P1604-C2, C3 and C4, respectively. Panels [D-F] represent NPP derived from ^{14}C incubations (solid lines) and $NPP_{G/G}$ from dilution incubations (dashed lines). Panels [G-I] show new production (from ^{15}N incubations; solid lines) and export production from sediment traps (dashed lines). Panels [J-L] show mixed layer NCP_{Prior}. Panels [M-O] show instantaneous air-sea biological O_2 flux. Panels [P-R] represent calculated GPPs during the diel cycles as measured by NCP_{inst}. Note changes in scales and units as indicated by the axis labels. Data in panels D-I are integrated over 24 h and mixed layer depth. Data in panels A-C and J-R are integrated over 30-min intervals.

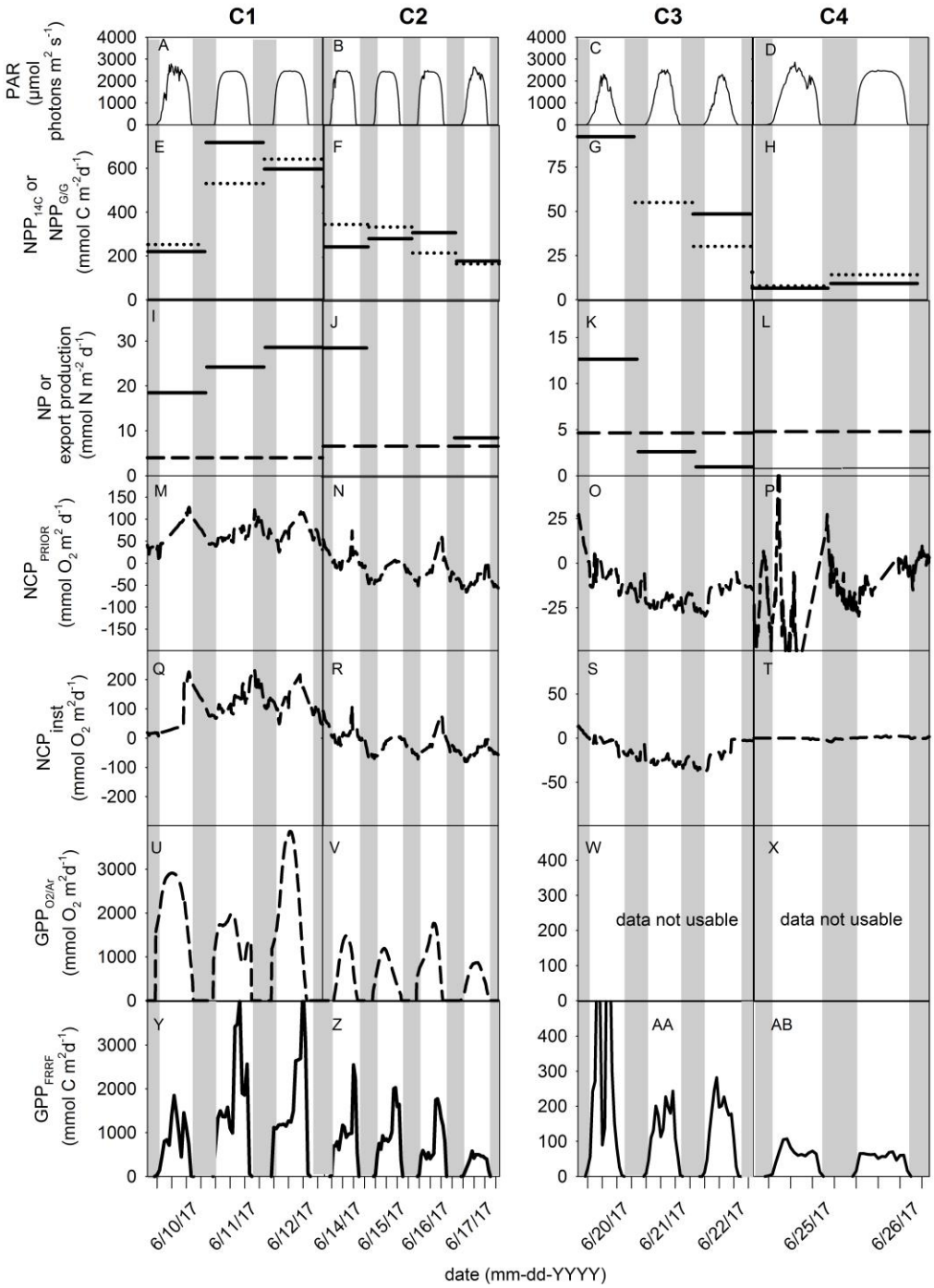

Figure 4.

Chronology of primary production estimates during P1706. Panels [A-D] depict the light intensity during the for cycles P1706-C1 to C4, respectively. Panel [E-H] represent NPP derived from ^{14}C incubations (solid lines) and the $NPP_{G/G}$ from dilution incubations (dashed lines). Panels [I-L] show new production (from ^{15}N incubations) and export production from sediment traps. Panels [M-P] represent net community production measured with weighted k. Panels [Q-T] show net community production calculated using instantaneous k. Panels [U-X] represent calculated gross primary production from instantaneous NCP. Panels [Y-AB] represent gross primary production measured by FRRF. Note changes in scales and units as indicated by the axis labels. Data in panels E-P are integrated over 24 h and the mixed layer depth. Data in panels A-D and M-AB are integrated over 30-min intervals.

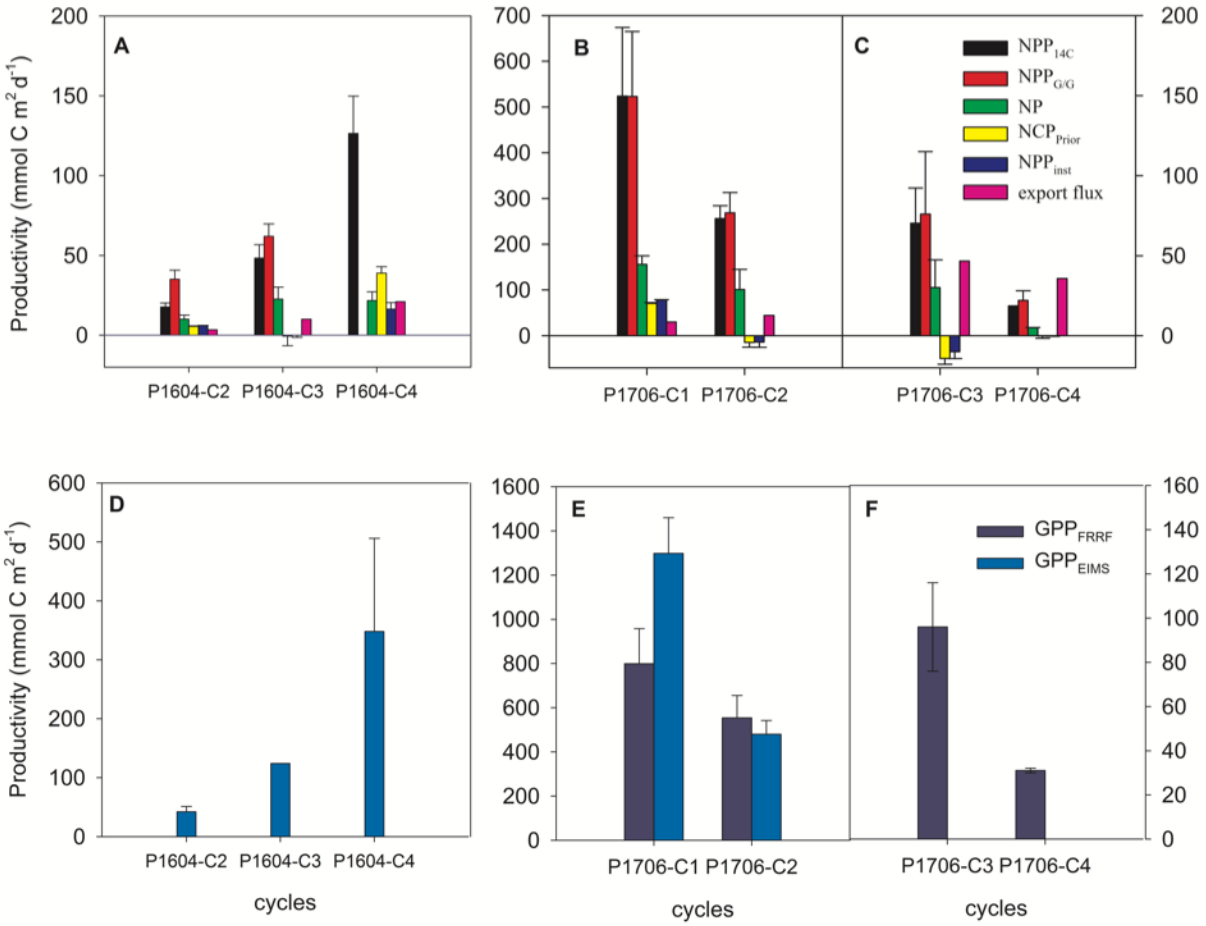

Figure 5. Summary of all production estimates. Data are normalized to carbon units. Note difference in scales between the graph panels.

[JGR-Oceans]

Supporting Information for

Lagrangian studies of marine production: a multi-method assessment of productivity relationships in the California Current Ecosystem upwelling region

Sven A Kranz[1,*], Seaver Wang[2], Thomas B Kelly[1], Michael R Stukel[1,3], Ralf Goericke[4], Michael R. Landry[4], Nicolas Cassar[2]

[1]Dept. of Earth, Ocean & Atmospheric Sciences, Florida State University, Tallahassee, FL

[2]Division of Earth and Ocean Sciences, Duke University, Durham, NC

[3]Center for Ocean-Atmospheric Prediction Studies, Florida State University, Tallahassee, FL

[4]Integrative Oceanography Division, Scripps Institution of Oceanography, La Jolla, CA

Contents of this file

Introduction: The supporting data and information presented here is provided to allow the reader to get more detailed information on methods and results presented in the main manuscript.

Chlorophyll analysis: Samples were filtered onto GF/F filters and subsequently placed into culture tubes containing 90% acetone and placed in a freezer. The fluorescence of the samples was read on a fluorometer (Turner 10AU) after 24 to 48 hours of extraction. The samples were subsequently acidified to degrade chlorophyll to phaeopigments (i.e. non-photosynthetic pigments). The readings prior to and after acidification are used to calculate concentrations of both chlorophyll a and phaeopigments (i.e. phaeophytin). In addition, continuous surface (c. 5m) chlorophyll a readings were taken using the ship-board flow through fluorometer.

Gross production using variable Chl-a fluorescence: The FRRF measures single turnover fluorescence induction curves including a relaxation phase. Fluorescence light curve measurements (FLC) were conducted which lasted approximately 30 minutes. A 12-minute dark adaptation time was chosen with a 60 second weak light acclimation (i.e. 20 µmol photons m^{-2} s^{-1}) prior to taking the variable fluorescence measurement. The instrument's measurement chamber was temperature regulated to match the surface mixed layer. Each sample was exchanged with fresh seawater from the ship's uncontaminated flow-through system using an automated peristaltic pump. The ship's flow-through system ran continuously at > 4 L min^{-1} ensuring that the sample reflected the contemporaneous phytoplankton community.

The excitation setting was set to of 100 flashlets on a 2 µs pitch and a relaxation phase of 40 flashlets on a 60 µs pitch. The gain of the instrument was set to "auto" to adjust for the variation in biomass and fluorescence signal throughout the cruise. Excitation was provided by 3 LEDs (i.e. 450 nm, 530 nm and 625 nm). Here we only used the single 450 nm Chl *a* excitation to evaluate our data. High resolution FLCs with 19 light steps covering light intensities of 22, 49, 81, 118, 163, 216, 279, 353, 442, 547, 671, 819, 995, 1204, 1451, 1745, 2094, 2508, 3000 µmol photons $m^{-2}s^{-1}$ were conducted.

Our correlation of F_0 vs. Chl *a* indicated an offset at which base fluorescence was still elevated under a zero Chl a concentration. In order to re-calculate RCII in the water column we used a baseline corrected F_0 at a given Chl *a* concentration to adjust RCII to the chlorophyll concentration in the mixed layer water column.

The ratio of Reaction center to chlorophyll η_{PSII} (mol RCII: mol Chl *a*) was calculated based on RCII (Oxborough et al., 2012) taken during nighttime and the measured Chl *a* concentration during those times

Table S1. Description of terms used in the FRRF measurements.

Terms associated with the saturation phase of a single turnover (ST) FRR measurement		
Term	**Description**	**units**
$C_{(P, J \text{ or } L)}$	fraction of RCII in the closed state estimated as 1 – qP, 1 – qJ or 1 – qL	dimensionless
E	incident photon irradiance (photon flux density)	µmol photons m^{-2} s^{-1}
F’	fluorescence at zeroth flashlet of a single turnover measurement when C > 0	unitless
Fo’	Base fluorescence under ambient light	unitless
$F_{m(')}$	maximum fluorescence when C = 1(under ambient light)	unitless
F_o	fluorescence at zeroth flashlet of an ST measurement when C = 0 (under ambient light)	unitless
F_q'	$F_m' – F'$	unitless
F_q'/F_m'	fluorescence parameter providing an estimate of □PII under ambient light; ($F_m' – F'/ F_m'$)	dimensionless
$F_{v(')}$	$F_{m(')} – F_{o(')}$	unitless
$F_{v(')}/ F_{m(')}$	fluorescence parameter providing an estimate of □PII when C = 0 (under ambient light)	dimensionless
K_a	Instrument type-specific constant	m^{-1}
ϕ_{PII}	PSII efficiency; Estimated as F_q'/F_m'	dimensionless
η_{RCII}	RCII to Chl *a* ratio	unitless
NCP_{NSV}	normalized Stern-Volmer non-photochemical quenching coefficient, $NPQN_{SV}= (F_m'/F_v') – 1$	
Φe:c	Electron to carbon conversion, calculated as $\Phi e{:}\,c = (486 \cdot NPQ_{NSV} + 1854) * \eta_{RCII}$	unitless
oF'	fluorescence from open centers under ambient light $oF' = (F_m \text{ x } F_0)/ (F_m- F_0) * (Fq'/F_m)$;	unitless
JV_{PSII_abs}	PSII flux per unit volume	electrons (RCII m^{-3}) s^{-1}
qP, qJ and qL	Fq/Fv - the fraction of RCII in the open state	dimensionless
σ_{PII}	absorption cross section of PSII photochemistry	m^2 $PSII^{-1}$
$\sigma_{PII'}$	absorption cross section of PSII photochemistry under ambient light	m^2 $PSII^{-1}$

Table S2. Bio/physico/chemical properties of the mixed layer during each day of a cycle as well as mean and standard error of the mean for each cycle. Prior to the termination of a cycle the water column properties were measured, these are indicated as "final". Temperature (Temp; [°C]), mixed layer depth (MLD; [m]), Phosphorus (PO_4^{3-}; [µM]), Silicate (Si; [µM]), Nitrite (NO_2^-; [µM]), Nitrate (NO_3^-; [µM]), Ammonia (NH_4^+; [µM]) and chlorophyll concentration; [Chl a ,µg L^{-1}]), POC and PON [ug L^{-1}], POC:PON [mol:mol].

Cycle	Temp	MLD	PO_4	dSi	NO_2	NO_3	NH_4	Chl *a*	POC	PON	C:N
	[°C]	[m]	[µM]	[µM]	[µM]	[µM]	[µM]	[µg L^{-1}]	[µg L^{-1}]	[µg L^{-1}]	mol:mol
P1604											
Cycle 1-1	17.44	13.04	0.23	1.58	0.00	0.05	0.02	0.07	41	6.99	6.84
Cycle 2-1	15.31	68.08	0.33	2.01	0.01	0.13	0.00	0.14	35.44	5.44	7.59
Cycle 2-2	15.31	70.96	0.34	2.02	0.00	0.14	0.00	0.12	34.86	5.74	7.09
Cycle 2-3	15.42	73.72		1.75	0.00	0.01	0.00	0.13	34.75	5.54	7.31
Cycle 2-4	15.53	67.34	0.27	2.10	0.00	0.00	0.01	0.11	34.63	5.34	7.56
Mean	***15.39***	***70.03***	***0.31***	***1.97***	***0.00***	***0.07***	***0.00***	***0.13***	***34.92***	***5.52***	***7.38***
SEM	***0.05***	***1.46***	***0.02***	***0.08***	***0.00***	***0.04***	***0.00***	***0.01***	***0.179***	***0.08***	***0.11***
Cycle 3-1	13.69	17.57	0.61	6.01	0.15	4.44	0.16	0.89	124.6	27.93	5.20
Cycle 3-2	13.91	18.02	0.60	6.03	0.15	3.59	0.11	1.06	65.76	16.67	4.60
Cycle 3-3	13.95	15.89	0.58	6.71	0.13	3.49	0.08	0.99	177.9	40.91	5.07
Cycle 3-4	14.29	12.91	0.50	6.00	0.12	2.54	0.05	0.93	94.7	20.18	5,47
Mean	***13.96***	***16.10***	***0.57***	***6.19***	***0.14***	***3.52***	***0.10***	***0.97***	***115.7***	***26.42***	***5.08***
SEM	***0.12***	***1.16***	***0.02***	***0.17***	***0.01***	***0.39***	***0.02***	***0.04***	***47.89***	***10.74***	***0.36***
Cycle 4-1	14.53	14.86	0.41	4.32	0.05	0.63	0.61	4.07	455.59	85.94	6.18
Cycle 4-2	14.78	11.86	0.36	5.61	0.06	0.68	0.34	4.22	508.3	98.78	6.00
Cycle 4-3	14.78	13.33	0.45	6.16	0.08	0.97	0.53	2.66	393.4	78.63	5.83
Cycle 4-4	14.50	12.90	0.49	7.03	0.10	1.51	0.49	4.09	466.0	92.24	5.89
Mean	***14.65***	***13.24***	***0.43***	***5.78***	***0.07***	***0.95***	***0.49***	***3.76***	***455.8***	***88.9***	***5.98***
SEM	***0.08***	***0.62***	***0.03***	***0.57***	***0.01***	***0.20***	***0.06***	***0.37***	***23.7***	***4.3***	***0.07***
P1706											
Cycle 1-1	13.60	19.90	0.89	11.00	0.27	10.41	0.35	7.34	72.23	361.9	5.84
Cycle 1-2	13.20	20.70	0.45	5.72	0.21	5.31	0.23	13.49	116.4	582.3	5.83
Cycle 1-3	13.20	22.80	0.51	5.84	0.24	5.72	0.51	8.02	90.00	431.8	5.59
Cycle 1-final	12.80	22.80	0.55	5.16	0.28	6.62	0.85	9.62	85.94	464.3	6.30
Mean	***13.20***	***21.55***	***0.60***	***6.93***	***0.25***	***7.02***	***0.49***	***9.62***	***91.13***	***460.0***	***5.89***
SEM	***0.16***	***0.74***	***0.10***	***1.36***	***0.02***	***1.16***	***0.13***	***1.38***	***9.22***	***46.00***	***0.14***
Cycle2-1	13.10	25.40	0.59	1.28	0.32	6.72	0.53	4.75	476.8	85.68	6.49
Cycle2-2	13.10	27.50	0.78	3.49	0.35	8.18	0.72	3.43	308.9	56.98	6.32
Cycle2-3	13.30	31.40	0.75	3.51	0.36	7.79	0.65	3.27	306.0	56.62	6.31
Cycle2-4	13.40	33.60	0.78	3.92	0.35	7.71	0.72	2.39	264.9	46.84	6.60
Cycle2-final	13.50	33.10	0.83	4.48	0.35	7.68	1.40	1.68	199.17	37.77	6.15
Mean	***13.33***	***31.40***	***0.79***	***3.85***	***0.35***	***7.84***	***0.87***	***2.69***	***311.16***	***56.77***	***6.37***
SEM	***0.08***	***1.24***	***0.01***	***0.21***	***0.00***	***0.10***	***0.16***	***0.36***	***45.91***	***8.05***	***0.08***
Cycle3-1	15.00	18.90	0.53	2.76	0.22	4.19	0.15	1.79	215,39	38.35	6.55
Cycle3-2	15.20	21.20	0.39	3.05	0.10	1.61	0.21	0.60	104.46	17.54	6.94
Cycle3-3	15.50	36.80	0.34	3.03	0.06	1.00	0.16	0.44	57.34	9.95	6.72
Cycle3-final	15.40	46.00	0.34	2.62	0.07	0.92	0.45	0.34	70.08	12.55	6.51
Mean	***15.28***	***30.73***	***0.40***	***2.87***	***0.11***	***1.93***	***0.24***	***0.79***	***111.82***	***19.6***	***6.68***
SEM	***0.11***	***6.46***	***0.04***	***0.11***	***0.04***	***0.77***	***0.07***	***0.34***	***35.9***	***6.44***	***0.10***
Cycle4-1	15.30	21.40	0.55	0.29	0.21	2.41	1.39	0.30	94.13	17.24	6.37
Cycle4-2	15.70	19.00	0.61	0.70	0.22	3.13	1.63	0.23	87.18	14.98	6.78
Cycle4-final	16.30	15.10	0.62	0.88	0.20	3.12	2.16	0.20	87.63	17.41	5.87
Mean	***15.77***	***18.50***	***0.59***	***0.62***	***0.21***	***2.89***	***1.73***	***0.24***	***89.64***	***16.54***	***6.34***
SEM	***0.29***	***1.84***	***0.02***	***0.17***	***0.01***	***0.24***	***0.23***	***0.03***	***2.24***	***0.78***	***0.26***

Table S3. Production estimates for each day of a cycle. Net primary production using ^{14}C (NPP_{14C}), Net Primary production using the dilution experiment ($NPP_{G/G}$), New Production using the ^{15}N incubation method, Net community production using a weighted k (NCP_{PRIOR}). Net

community production using an instantaneous k (NCP_{RT}), average respiration during the night using the NCP_{RT} analysis (NCP_{RESP}), Gross primary production using the NCP_{RT} analysis ($GPP_{O2/Ar}$), Gross primary production using the FRRF data. All data are given in (mmol C m^{-2} d^{-1}). ND indicates no measurement was performed, X indicates that data were not usable.

	NPP_{14C}	**$NPP_{G/G}$**	**NP_{15N}**	**NCP_{Prior}**	**NCP_{RT}**	**NCP_{Resp}**	**$GPP_{O2/Ar}$**	**GPP_{FRRF}**
P1604								
P1604-cycle 2								
2-1	22.34	44.42	15.95	5.79	9.74	55.08	70	ND
2-2	16.72	24.31	8.25	5.74	7.18	63.06	47	ND
2-3	13.97	36.32	7.68	5.00	1.14	53.61	33	ND
P1604-cycle 3								
3-1	36.10	49.41	14.39	-10.75	-2.28	X	22	ND
3-2	44.52	60.29	14.45	0.39	0.11	X	X	ND
3-3	64.42	76.25	39.72	8.61	1.78	130	149	ND
P1604-cycle 4								
4-1	149.79	ND	28.76	43.46	12.32	288	228	ND
4-2	103.02	ND	17.02	35.49	20.41	632	608	ND
4-3	113.09	ND						ND
P1705								
P1705-cyle 1								
1-1	219.62	252.20	122.35	58.62	76.99	1381	1212	519
1-2	718.00	731.89	159.32	56.90	77.84	1128	813	1136
1-3	596.95	588.11	188.79	61.18	78.70	1327	1220	1148
P1705-cyle 2								
2-1	247.43	349.58	189.6	7.98	15.62	852	385	789
2-2	284.09	337.47		-14.26	-21.07	494	390	808
2-3	311.33	219.51	57.59	-9.01	-12.90	479	540	645
2-4	182.21	170.41	57.59	-33.65	-38.72	394	287	281
P1705-cyle 3								
3-1	92.33	177.07	83.80	-3.11	-4.16	39	X	172
3-2	ND.	55.42	20.32	-17.37	-20.90	47	X	81
3-3	48.45	30.02	6.72	-13.17	-14.12	92	X	92
3-4			6.377	-13.67	-2.74	97	X	
P1705-cyle 4								
4-1	13.1	15.60	5.17	-2.35	-0.42	85	X	37
4-2	18.57	28.40	5.49	1.62	0.57	45	X	34
4-2			5.52	0.17	0.07	45	X	

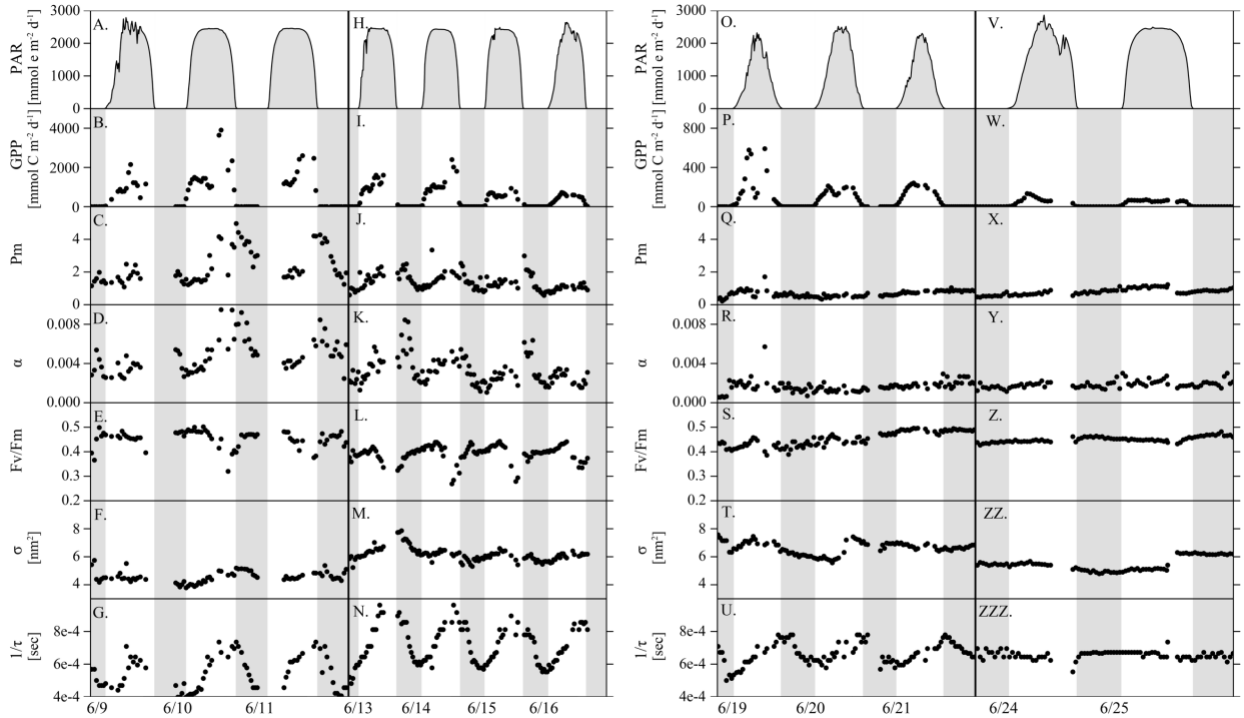

Figure S1. Chronology of photophysiological parameters during the CCE Process cruise P1706. Panels A, H, O, V show the diel cycles of light intensity. Panels B, I, P, W show the diel cycle of estimated GPP. Panels C, J, Q, W are maximum photosynthetic rates in [electrons $RCII^{-1}$ s^{-1}]. Panels D, K, R, Y show the changes of the slope of photosynthetic activity under low light intensities. Panels E, L, S, Z show the photosynthetic quantum yield. Panels F, M, T, ZZ show the absorption cross sectional area of the photosystem. Panels G, N, U, ZZZ show the rate of electron transport through the photosystem in the dark-adapted stage.